Project ID 37877

Design Build Fly of a Radio-Controlled Aircraft to Demonstrate Urban Air Mobility

A Major Qualifying Project Report
Submitted to the Faculty of the
WORCESTER POLYTECHNIC INSTITUTE
in Partial Fulfillment of the Requirements for the
Degree of Bachelor of Science
in Aerospace Engineering

Submitted by:

Elias Monzayet
Carson Murphy
Bridget Muturi
Jack Robertson
Troy Santopadre
Wesley Schultz
Richard Shaw
Regina Valencia

April 24, 2024

Submitted to:
Zhangxian Yuan, Advisor
Assistant Professor, Aerospace Engineering Department
WPI

Abstract

Under the theme of urban mobility, a radio-controlled aircraft was created with the following configuration: single front-mounted motor, high wing, taildragger, and conventional tail. The aircraft had to fit within a 2.5 foot wide parking area; thus, the aircraft was designed to be able to rotate its 4.9 foot wide wing. Inserts and restraints were designed to carry payloads for three payloads. This included a crew-only mission; a crew, patient, and medical supply cabinet mission; and a crew and passenger mission. Overall, the aircraft was able to transport 2 pounds of payload during the second mission and 10 passengers for the third mission. During the competition, the team placed 61st out of 107 participants, successfully completing the ground mission and the first flight mission.

Acknowledgments

The MQP team would like to express their gratitude to the following people who contributed to the successful completion of our project. Their assistance and expertise were essential in our project's progress towards achieving our goals.

- Project Advisor Professor Zhangxian Yuan for his guidance and support thought the project.
- The Aerospace department, for their financial support throughout the project and organizing travel logistics for our travel team.
- Randy Holtgrefe for providing guidance and feedback on our plane as well as donating aircraft components to us.
- Central Massachusetts Radio Control Modelers for offering their field for our plane tests and providing critique and knowledge in building RC aircraft.
- Professor David Olinger for providing guidance on wind tunnel testing and advice from previous Design Build Fly competition.
- The AIAA Chapter and the following underclassmen members for their contribution to the project:
    - Sophia Wong
    - Tyler Allison
    - Nathan Barry
    - Cameron Best
    - Ian Cody

Table of Authorship

Section	Author(s)
1. Introduction	RV
1.1 MQP Objectives, Methods, and Standards	CM
1.2 Project Goals	CM
1.3 Project Management	RV
1.4 MQP Timetable	RV
1.5 MQP Budget	RS
1.6 Safety and Regulatory Compliance	CM
2. Conceptual Design	JR
2.1 Technical Requirements	TS, JR
2.2 Mission Requirements	TS, JR
2.3 Mission Staging	JR
2.4 Flight Path Requirements	JR
2.5 Mission Sequence and Score	JR
2.5.1 Flight Mission 1: Delivery Flight	TS, JR
2.5.2 Flight Mission 2: Medical Transport Flight	TS, JR
2.5.3 Flight Mission 3: Urban Taxi Flight	TS, JR
2.5.4 Ground Mission	JR
2.6 Subsystem Design Requirements	BM, RV, TS, EM
2.7 Mission Sensitivity Analysis	EM
2.8 Aircraft Configuration	JR

2.8.1 Wing Configuration	JR
2.8.2 Tail Configuration	TS, JR
2.8.3 Propulsion Configuration	JR
2.8.4 Landing Gear Configuration	JR
2.8.5 Selected Configuration	JR
3.1 Initial Weight Estimation	BM
3.2 Aerodynamic Analysis	BM, JR
3.2.1 Airfoil Selection	BM, JR
3.2.2 Wing Sizing and Geometry	BM, JR
3.2.3 Tail Analysis	TS, EM
3.2.4 Lift and Drag Analysis	BM
3.2.5 Pitch Analysis	TS, EM
3.2.6 Take-off Distance	BM
3.3 Controls Analysis	TS, EM
3.3.1 Neutral Point Calculations	TS, EM
3.3.2 Control Surface Sizing	TS, EM
3.3.4 Trim Analysis	TS, EM
3.4 Propulsion Analysis	EM
3.4.1 Battery Analysis	EM
3.4.2 Motor and Propeller Sizing	EM
3.5 Structural Analysis	RS
3.5.1 Fuselage Sizing and Design	RV

3.5.2 Wing Deflection Analysis	RS
4.1 Dimensional Parameters	All
4.2 ANSYS Wing Analysis	CM
4.3 Controls	TS, EM
4.3.1 Ailerons & Flaps	TS, EM
4.3.2 Elevator, Rudder and Rear Landing Gear	TS, EM
4.3.3 Throttle Control	TS, EM
4.4.1 Fuselage Integration	RS
4.4.2 Wing Integration	RS
4.4.3 Tail Integration	RS
4.4.4 Landing gear Integration	RS
4.4.5 Mission Inserts Integration	RV
4.5 Flight Performance	BM
5 Manufacturing Plan	RV
5.1.1 Laser Cutting	RV
5.1.2 3D Printing	RV
5.1.3 Adhesives	RV
5.1.4 Monokote	RV
5.2 Manufacturing Overview	RV
5.2.1 Wing Construction	RV
5.2.2 Fuselage Construction	RV
5.2.3 Tail and Tail Boom Construction	RV

5.2.4 Mission Inserts Construction	RV
6 Testing Plan	EM
6.1 Sub-System Testing	EM
6.1.1 Aerodynamic Testing	BM
6.1.2 Propulsion Testing	EM
6.1.3 Structural Testing	RS
6.1.3.1 Firewall Testing	RS
6.1.3.2 Wing Loading	EM
6.1.3.3 CG Test	EM
6.1.4 Control Testing	EM
6.1.4.1 Servos Configuration Testing	EM
6.1.4.2 Failsafe Test	EM
6.2 Flight Testing	EM
6.2.1 Flight Testing Checklist	JR
6.3 Flight Testing Results	EM
6.3.1 First Flight Test	EM
6.3.2 Second Flight Test	EM
6.3.3 Third Flight Test	EM
6.3.4 Fourth Flight Test	BM
6.3.5 Fifth Flight Test	BM
7 Conclusion	BM
7.1 Summary	BM

7.2 Conclusions	BM
7.3 Recommendations for Future Work	BM, RS,TS
7.4 Project Broader Impacts	BM
8.4 APPENDIX D: Aircraft Drawing Package	RV

Authorship Table initials

Name	Initials
Elias Monzayet	EM
Carson Murphy	CM
Bridget Muturi	BM
Jack Robertson	JR
Troy Santopadre	TS
Wesley Schulz	WS
Richard Shaw	RS
Regina Valencia	RV

Table of Contents

Table of Figures

Table of Tables

Nomenclature

Variable Name	Symbol	Unit
Reynolds Number	Re	Unitless
Density	ρ	$\frac{slug}{ft^3}$
Velocity	V	$\frac{ft}{s}$
Chord	c	feet
Kinematic Viscosity	μ	$\frac{lb-s}{ft^2}$
Lift Coefficient	C_L	Unitless
Weight	W	Pounds
Total Weight	W_{total}	Pounds
Crew Weight	W_{crew}	Pounds
Battery Weight	$W_{battery}$	Pounds
Payload Weight	$W_{payload}$	Pounds
Empty Weight	W_{empty}	Pounds
Required Lift Coefficient	$C_{L_{required}}$	Unitless
Wing Area	S	ft^2
Battery Mass Fraction	BMF	Unitless
Climb Time	T_{climb}	Hours
Motor Power	P_{motor}	Watts
Specific Energy	E_{sb}	Watt-hours
Battery Efficiency	n_b	Unitless
Aircraft Range	R	Feet
Gravity	g	$\frac{ft}{s^2}$
Propulsion Efficiency	n_p	Unitless
Angle of Attack	AOA or Alpha or α	Degrees
Drag Coefficient	C_D	Unitless
Moment Coefficient	C_M	Unitless
Quarter-Chord Moment Coefficient	$C_{M_{\frac{C}{4}}}$	Unitless
Parasitic Drag Coefficient	C_{D_0}	Unitless
Pi	π	Unitless
Aspect Ratio	AR	Unitless

Oswald Efficiency Factor	e	Unitless
Cruise Weight	W_c	Pounds
Ground Roll Angle of Attack	$\alpha_{ground\ roll}$	Degrees
Thrust	T	Pounds-Force
Drag	D	Pounds-Force
Lift	L	Pounds-Force
Takeoff Distance	$S_{ground\ roll}$	Feet
Static Margin	SM	Unitless
X-Position of Neutral Point	X_{NP}	Inches
X-Position of Center of Gravity	X_{CG}	Inches
Mean Aerodynamic Chord	MAC	Inches
Mass Moment of Inertia	I	in^2
Outer Diameter	d_o	Inches
Inner Diameter	d_i	Inches
Maximum Deflection	δ_{max}	Inches
Load	w	Pounds
Length	l	Inches
Elastic Modulus	E	KSI
Length of Distributed Load	x	Inches
Bending Moment	M	Pound-force-inches
Shear Force at Specified Location	V	Pound-force
First Moment of Area	Q	in^3
Shear Stress	τ	KSI
Thickness	t	Inches

1 Introduction

This document represents the MQP report of the 2023-2024 Worcester Polytechnic Institute (WPI) Design, Build, Fly (DBF) team. WPI, under the team name Project Phoenix, has created and tested a radio-controlled plane that will perform four urban air mobility themed missions: a crew-only flight; a crew, patient, and medical supply cabinet flight; a crew and passenger flight; and a ground configuration change mission. The aircraft must follow certain requirements including a wingspan that cannot exceed 5 feet and a parking configuration that is 2.5 feet wide. Additionally, the aircraft must takeoff within 20 feet.

The aircraft design process was divided into 3 phases: conceptual design phase, preliminary design phase, and detailed design phase. During the first phase, the team divided the mission requirements into sub-system requirements, conducted a sensitivity analysis, and outlined an aircraft configuration. During the second phase, the team conducted several analyses under aerodynamics, controls, propulsion, and structures; this informed the team on how the aircraft would be designed. During the third phase, the team finalized the structural design and integration of the aircraft. Afterwards, a manufacturing plan was established using several manufacturing processes. Once the aircraft was completed, a flight plan was established to test its performance, in which the plane would go through a run without payload, a Mission 1 run, a Mission 2 run, and a Mission 3 run at the minimum. Additional flights were scheduled to test modifications.

Project Phoenix's aircraft was designed as a conventional tail, high-wing, single motor, taildragger plane. The design was able to accommodate the required crew and payload and had a maximum volume for 10 passengers to fit. For materials, the team decided on a primarily wooden structure, with lightweight woods being used (e.g., balsa, lite plywood, basswood, and lauan plywood). The wing of the aircraft had a carbon fiber spar; the tail was connected to the fuselage with two carbon fiber rods as well. The plane went through numerous changes in terms of choice of materials, fuselage design, tail control surface sizing, and the creation of a battery compartment. The team analyzed the design through various software including MATLAB, XFLR5, SolidWorks, and ANSYS; the team also conducted hand-calculations and experimental tests.

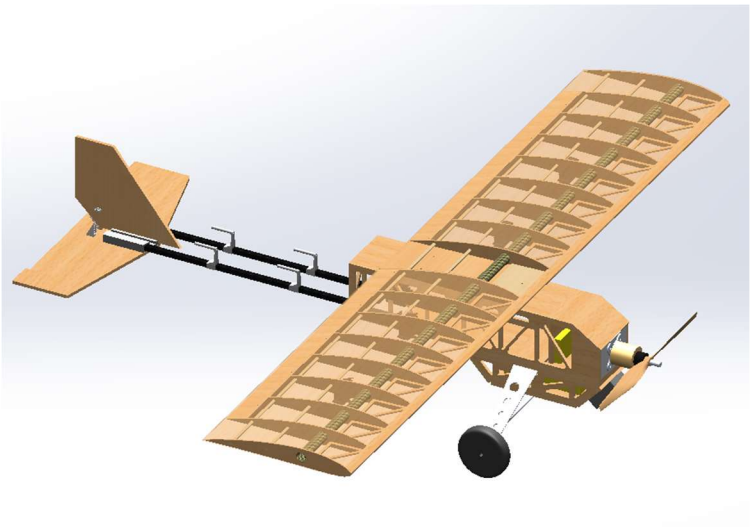

Figure 1: Project Phoenix's aircraft.

1.1 MQP Objectives, Methods, and Standards

The MQP serves as a student's senior engineering capstone project at WPI. This is a team-based project designed to showcase a student's learning and experience in their specific area of study throughout their time at WPI. This project integrates the aerospace related knowledge acquired through our course work with of a variety of software applications including, but not limited to, MATLAB, SolidWorks, ANSYS, and XFLR5. The use of various software enhanced the accuracy of the initial design and the modification of numerous design iterations. This project successfully meets the MQP learning outcomes by combining the software listed above with the project goals outlined in Section 1.2 to create a radio-controlled aircraft that is designed to meet the mission requirements for the DBF competition.

1.2 Project Goals

The goal of this project is to design an RC aircraft that can achieve flight with three different payloads under the theme of urban mobility. To achieve this goal, the project was broken down into numerous smaller goals that were achieved over the course of the year in preparation for the competition in April of 2024. The goals of the project are listed below.

1. Aircraft Design Process
    a. Software training to ensure a requisite level of expertise.
    b. Sensitivity analysis to determine the most important aspect of each mission to help optimize scoring.

c. Conceptual design to define what major components should look like: tail configuration, landing gear configuration, number of motors, etc.
d. Preliminary design to create of a 3D model of the aircraft using Computer-Aided Design software to determine how to best integrate different aspects of the conceptual design.
e. Detailed design to decide what each component of the aircraft will look like, what material it will be made out of, and how they will fit together.
f. Design review to critically analyze the current design used to determine how to improve the theoretical and experimental characteristics of the aircraft.

2. Manufacturing
    a. Creation of prototype 1 to visualize the aircraft based of results from detailed design.
    b. Creation of prototype 2 to make modifications based off the results from the design review and to test in flight.
    c. Creation of prototype 3 to make modifications based off the results from the second design review and to test in flight with payloads.
    d. Creation of final model to use for the DBF competition.
3. Testing and Analysis
    a. Scale wing simulation testing to determine which airfoil(s) have the most desirable characteristics.
    b. Wind tunnel testing to confirm scale wing simulations with experimental data.
    c. Glide testing to ensure the lift characteristics and stability of the aircraft are desirable using foam material.
    d. Flight testing without a payload to ensure the aircraft is stable, controllable, and has the expected levels of performance.
    e. Flight testing with a payload to determine exactly what payload capacity the aircraft is capable of carrying safely in preparation for the competition missions.
    f. Ground mission testing to ensure the fully constructed aircraft is capable of completing the ground mission as defined by the DBF rules.

1.3 Project Management

The MQP team had 8 seniors; in addition, 5 underclassmen joined to create a DBF team. the WPI DBF team had 13 members, with 61.5% of the team being seniors and 38.5% of the team being underclassmen. Additionally, one faculty member from WPI's Aerospace Engineering Department served as an advisor for the team. The team was divided into 5 sub-teams, detailed in Figure 2; the general responsibilities of each sub-team and the team at large are listed in Table 1.

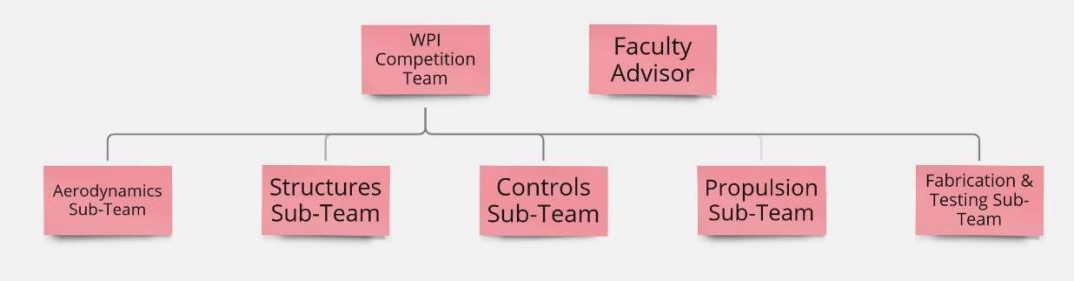

Figure 2: Team organizational structure.

Table 1: Sub-group breakdown and responsibilities

Structures	Aerodynamics	Propulsion	Controls & Stability	Fabrication
-Structural analysis -Rotating wing mechanism -Fuselage design (internal)	-Wing planform shape design -Lift and Drag Calculations -Fuselage design (external)	-Motor and Propeller selection	- Control Surface Design -Neutral Point Calculation -Control Surface Actuation -Trim Analysis -Servo Selection	-Manufacturing of plane

1.4 MQP Timetable

In accordance with deadlines set by the DBF competition, the Gantt chart in Table 2 details the major milestones that the team planned to meet. The dates are divided into four sections, which include "Aircraft Design Process," "Manufacturing," "Testing/Analysis," and "Competition Deadlines." The gray section of the chart denotes WPI's official winter break, and the black lines represent the actual time spent.

Table *2* : MQP team Gantt chart

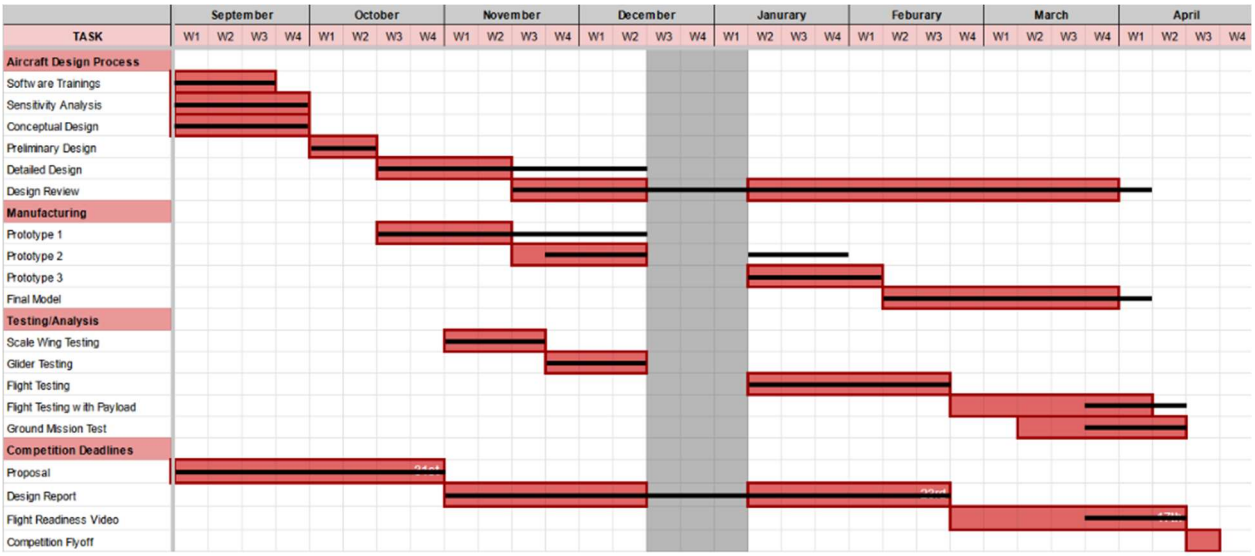

1.5 MQP Budget

WPI's Aerospace Engineering Department provided the Project Phoenix team with a budget of $2000 for the project. This money was used solely for the advancement of the aircraft construction. Other costs, such as those related to travel and living accommodation expenses for the competition, will be covered by WPI. As such, they are not included in the analysis of the team's budget. The travel budget will cover costs for flights and accommodation for up to 3 members of the team. Previous DBF teams at WPI had leftover materials that were used by this team to save money. This included a motor, electronic speed controller, and Monokote.
Table 3 shows the distribution of the budget so far. Structures required the highest allocation of the budget at 27.27%. This was higher than originally anticipated. The cost and amount of balsa wood was underestimated at the beginning of the project. The propulsion cost was lower than expected due to the team using a motor provided by WPI. With a subtotal of $1232.46, there is still $767.54 left over for the remainder of the project. This budget will go towards the construction of replacement parts to prepare for potential repairs required at the competition.

Table *3*: Categorical budget breakdown

Sub-team	Cost	Percentage of Budget
Structures	$545.38	27.27%
Propulsion	$369.64	18.48%
Controls	$227.44	11.37%
Misc.	$90.00	4.50%
Subtotal	$1232.46	61.62%

1.6 Safety and Regulatory Compliance

Throughout the design and testing phases, safety prevailed as a main priority for the team. The team's safety officer attended a lab safety training administered by the University's Environmental Health and Safety department. Throughout the manufacturing and testing phases, the team maintained safe lab practices by ensuring all combustible materials such as isopropyl alcohol, acetone, and epoxy, were stored in a fireproof flammables' cabinet. The lithium polymer batteries were stored in fireproof bags or boxes and charged only in the presence of a team member to reduce the risk and severity of a potential battery fire.

The team also ensured relevant laws and regulations were followed throughout the testing phase of the project. Specifically, Title 14 Code of Federal Regulations Part 89 was a main concern for the team [7]. These laws, taking effect just 3 weeks after the start of the project, drastically changed the regulations that governed test flights of the aircraft. All test flights of the aircraft were performed within an FAA Recognized Identification Area (FRIA) established in accordance with 14 CFR 89 C. This meant the team was not required to comply with the Remote ID regulations, as the remote ID capability is not required within an FRIA. The team is expecting the competition site to be deemed as an FRIA, however, the team has prepared equipment to comply with these regulations should the competition site not be deemed an FRIA by the Federal Aviation Administration.

2 Conceptual Design

This section of the report summarizes the initial phase of the aircraft design process, conceptual design. An overview of the competition and the requirements for the aircraft is first detailed, followed by the discussion of different aircraft components and the team's selection process on their configurations.

2.1 Technical Requirements

The competition rules defined the essential requirements the aircraft had to meet. Working under the scope of Urban Air Mobility, the competition flight missions required the aircraft to be capable of carrying internal payloads, taking-off within 20 feet of the start line, and complete a successful landing at the end of a given flight path. All aircraft within the competition will undergo a Technical Inspection, to ensure competition safety. The technical inspection will be completed by a designated contest technician who will:

1. Verify all components are adequately secured to the vehicle
2. Verify all hatches have a positive, mechanical latching method
3. Verify propeller structural and attachment integrity
4. Visually inspect the electronic wiring
5. Complete a radio range check
6. Verify all controls move in the proper sense
7. Check the general integrity of the payload system

In addition to the checks listed above, the aircraft must also pass a wing tip load test. During this test, the aircraft is subjected to the maximum takeoff weight that it was designed to handle, loading the heaviest payload and battery combination that is anticipated to be used during the various flight missions. The aircraft must complete this test in its flight configuration, and the maximum load achieved during this test cannot later be exceeded following the technical inspection. Considering these technical regulations will be crucial in designing an aircraft fit for competition and should be considered during all phases of the design process.

2.2 Mission Requirements

The mission requirements presented in the AIAA 2023-2024 rulebook require the design, construction, and testing of an aircraft that demonstrates Urban Air Mobility (UAM) missions

[1]. This portion of the competition comprises 3 flight missions, each with unique objectives, and a ground mission. All three missions require the aircraft to takeoff and land successfully. To simulate a UAM mission, the aircraft was required to meet some general specifications. The aircraft's wingspan may not exceed 5 feet and must be configurable to fit into a 2 ½ foot wide parking spot. The aircraft was also required to be able to carry 2 crew members, 2 EMTs, a patient in a gurney, and a medical supply cabinet. The aircraft crew, EMTs, patients, and passengers are wooden peg dolls as seen below:

Figure 3: Crew, EMTs, and passengers (left) and patient (right).

The aircraft's passenger compartment must feature a single, level horizontal floor for accommodating EMTs, the patient on a gurney, a medical supply cabinet, and passengers. All passengers, including the crew, EMTs, patient, and passengers, must be secured by restraint systems to prevent movement during taxiing, takeoff, flight, and landing. Teams are allowed to create an insert above the floor of the plane specific to each mission to assist with this objective. Furthermore, the patient must be securely fastened to the gurney. During medical transport missions, EMTs should be positioned alongside the patient on the gurney, with specific guidelines to ensure they do not touch each other, the patient, the gurney, or any part of the aircraft, except the floor or insert. The medical supply cabinet can be placed either forward or aft of the EMTs and patient. Passengers, according to the layout shown in Figure 4, must also be situated in the passenger compartment without touching each other or any part of the aircraft, except the floor or insert. Lastly, the crew, consisting of the pilot and co-pilot, should be seated on a horizontal plane, side-by-side, without physical contact with each other or any part of the

aircraft. The crew's horizontal plane does not need to be coplanar with the passenger compartment floor, and the crew must be positioned so that their heads are above the fuselage in front of the cockpit, as shown in Figure 6, so that the pilots may “see”. A solid bulkhead must be installed between the Crew and Passenger compartments, as depicted in Figures 4, 5, and 6.

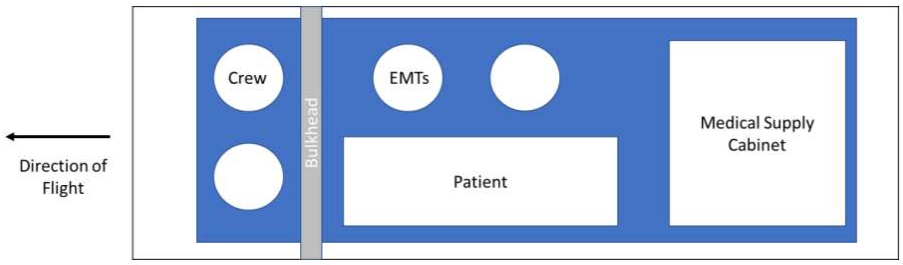

Figure 4: Example medical transport layout.

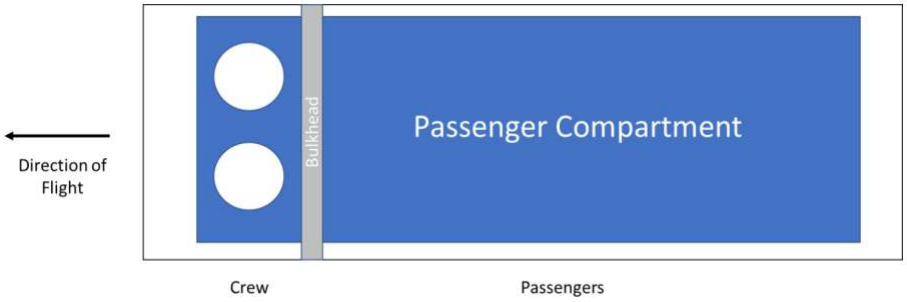

Figure 5: Example urban taxi mission layout.

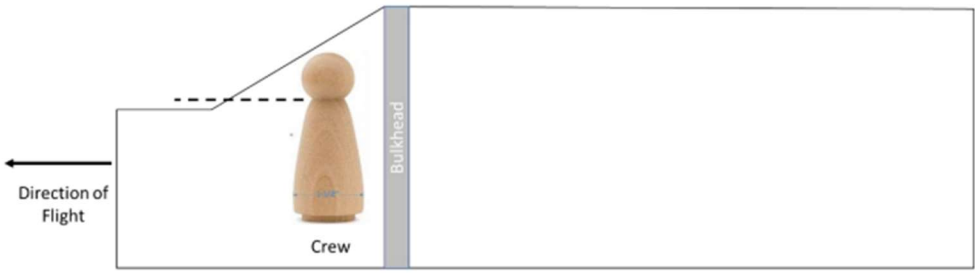

Figure 6: Positioning of crew relative to fuselage.

The plane must use the same configuration, excluding mission-specific payloads and inserts, to complete all missions.

2.3 Mission Staging

Prior to every flight attempt, the aircraft must be positioned in its parking configuration within the staging box with mission-crucial components such as the crew, EMTs, patient, gurney, medical supply cabinet, passengers, floor insert (optional), and propulsion battery pack(s) removed from the aircraft. If a team forgets necessary materials, they must leave the staging box and forfeit their flight attempt. The only people allowed in the staging box and Ground Mission area are the designated assembly crew member, the pilot, and the observer. The only person that is permitted to touch the aircraft within the staging box while preparing the aircraft for the mission is the assembly crew member. For each flight attempt, the propulsion battery will be inspected to verify that it had been approved during the technical inspection, and for Mission 2, the weight of the Medicine Supplies Cabinet payload will likewise be verified. Mission-specific items such as the Crew, EMTs, Patient, and maximum number of Passengers as declared during the tech inspection will be provided to the team for their respective missions.

During mission staging, the plane may not be picked up or rotated—it must remain upright and on its landing gear. The only exception to this mandate is granted if a team desires to check the balance of the plane by holding it from the wing tips, and in this case the assembly crew member may be assisted by the pilot or the observer. The staging of the aircraft must take no longer than 5 minutes.

2.4 Flight Path Requirements

According to the rulebook of the competition, all Flight Missions require an identical takeoff field length of 20 feet. Once the aircraft is airborne, it will follow a predetermined flight path involving a specific number of laps, each comprising two 180° turns, a 360° turn, and two 1000-foot straight sections, as illustrated in Figure 7.

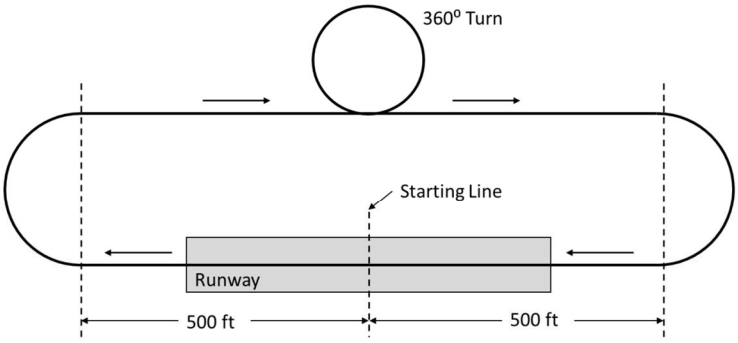

Figure 7: Course layout.

2.5 Mission Sequence and Score

The flight missions must be flown sequentially. A team may not attempt a score at a later mission until the team has accomplished a score for the preceding missions. This rule dictates that a team may not solely optimize their plane for the completion of a later mission without regarding their ability to complete earlier missions. After a successful attempt is completed for all three flight missions, only then may a team elect to attempt flight missions 2 and 3 a single, additional time for a chance at improving their score. The ground mission may be attempted at any time during the competition period. After successfully completing the ground mission, a team is granted a single, additional attempt to have the opportunity to improve their score.

Final scores for each team are based on the score assigned to the report that each team submits prior to the competition, the combined score generated by each team's mission performances, and each team's participation score. Participation score is based on a team's attendance of the competition, attempts made towards completing missions, and a team's completion of completed tech inspection. The report and mission scores for each team are multiplied together, and each team's respective participation score is added to the result to generate that team's final competition score. For all flight missions, the following stipulations apply:

- Each mission has a 5-minute window in which the laps must be completed with their respective payloads.
- A lap is completed when the plane passes over the start/finish line in the air, and landing is not included in the 5-minute window.

- The timer on the flight window starts when the aircraft throttle is advanced for the first takeoff—whether that takeoff attempt is successful or not.
- The aircraft must complete a successful landing to obtain a score for the mission attempt.

2.5.1 Flight Mission 1: Delivery Flight

The only necessary payload for the completion of the first mission is the crew members in the cabin of the aircraft. Teams must complete 3 laps of the flight path within a 5-minute flight window. The scoring for this mission is based on completion and there are no other factors. Equation 2.1 represents the scoring calculation for Flight Mission 1.

$$M1 = 1 \tag{2.1}$$

2.5.2 Flight Mission 2: Medical Transport Flight

The payload required for this mission is the crew, EMTs, patient on the gurney, and the medical supplies cabinet. The team will be timed on their completion of 3 laps of the flight path, but the mission must also be completed within a 5-minute flight window. Scoring for this mission is based on the weight of the medical supplies cabinet and the time taken to complete 3 laps. Equation 2.2 represents the scoring calculation for Flight Mission 2, with the numerator representing the team's result and the denominator representing the best team's result.

$$M2 = \frac{N\left(\frac{Payload\ Weight}{Time}\right)}{Max\left(\frac{Payload\ Weight}{Time}\right)} \tag{2.2}$$

2.5.3 Flight Mission 3: Urban Taxi Flight

The payload for this mission is the crew and the passengers. There will be a 5-minute flight window for this mission, and the number of laps recorded during that window will be recorded. Scoring for this mission is based on the number of passengers aboard the plane, the number of laps completed within the flight window, and the rated battery capacity of the propulsion battery. Equation 2.3 represents the scoring calculation for Flight Mission 3, with the numerator representing the team's result and the denominator representing the best team's result.

$$M3 = 2 + \frac{N\left(\frac{\#\ of\ Laps\ *\ \#\ of\ Passengers}{Battery\ Capacity}\right)}{Max\left(\frac{\#\ of\ Laps\ *\ \#\ of\ Passengers}{Battery\ Capacity}\right)} \quad (2.3)$$

2.5.4 Ground Mission

Similar to the typical mission staging requirements, teams will enter the ground mission with their aircraft in its parking configuration and without any payload, components, or propulsion batteries installed. Unlike during mission staging, installing a propulsion battery is not required, however, flight controls will still be tested following the completion of the mission. As with mission staging, the team's assembly crew member and pilot may enter the ground mission area, but only the assembly crew member may touch the aircraft, payload, and components. The ground mission has three segments, the first based on preparing the plane for flight mission 2, the second based on preparing the plane for flight mission 3, and the third based on returning the plane to its parking configuration with nothing on board. At the start of each segment, the ground mission judge will say "GO", at which point the timer starts and the assembly crew member may begin working on the plane.

The first segment of the ground mission concludes when the aircraft has been converted from its parking to its flight configuration and the assembly crew member believes that the payload and components for flight mission 2 are properly secured and says "STOP". Following this declaration from the assembly crew member, the ground mission judge will stop the timer and inspect the aircraft, verifying that the hatches and doors are secure. The pilot will then verify that the flight controls for the aircraft are functional.

The second segment of the ground mission begins when the ground mission judge says "GO" for a second time. At this point, the timer resumes, and the assembly crew member is tasked with removing the payload and components for flight mission 2 from the aircraft and replacing them with the payload and components for flight mission 3. When the assembly crew member believes that everything is secure, they will again say "STOP". At this point, the ground mission judge will again stop the timer, check that the hatches and doors are secure, and the pilot will test the flight controls.

For the third and final segment of the ground mission, the judge will again say “GO” and resume the timer. The assembly crew member must remove everything from the plane and return it to its parking configuration. This time when the assembly crew member says “STOP”, the total time is recorded by the ground mission judge. Scoring for this mission is based on the team’s time to complete the ground mission compared to the minimum time to complete the ground mission achieved by any team at the competition.

$$GM = \frac{Min(Mission\ Time)}{N(Mission\ Time)} \tag{2.4}$$

2.6 Subsystem Design Requirements

Table 4 below was created to ensure that the aircraft is constructed in accordance with the requirements outlined in the competition rules. Each requirement will be allocated to a sub-team as specified in Section 1.2. During the design process, the aircraft requirements will be verified through performing theoretical analysis and system level testing. The mission scoring breakdown in Table 5 describes aircraft characteristics that will be emphasized in the design process to maximize our scores for each mission.

Table 4: Aircraft Requirements

Requirement	Sub-Teams/ method of verification	Pass/Fail
The Aircraft wingspan cannot exceed 5 feet	Aerodynamics	Pass
The aircraft must fit inside a parking spot 2.5 feet wide.	Aircraft, CAD	Pass
The Aircraft cannot be rotary wing based or lighter than air.	Aircraft, CAD	Pass
Aircraft must be powered by the on-board propulsion system. No form of external assisted takeoff is allowed.	Propulsion	Pass
Structural components cannot be dropped from the plane during flight.	Aircraft	Pass
Aircraft must be propeller driven and electrically powered.	Aircraft	Pass

Must use commercial brushed or brushless electric motors.	Propulsion	Pass
Each aircraft must use a commercially produced propeller/blades.	Propulsion	Pass
Take off gross weight with payload must be less than 55 lbs.	Aircraft	Pass
Team must submit proof that the exact aircraft presented has been flown prior to the contest date.	Aircraft, Video submission	
The aircraft must remain the same as documented in the report.	Aircraft	Pass
The aircraft must have an externally accessible switch to turn on the radio control system.	Controls	Pass
One battery pack can be connected to the propulsion system where it would consist of one battery, one externally accessible arming fuse, one or more speed controllers (ESC), and one or more motors.	Propulsion	
If more than one battery pack is implemented for a single purpose, then the following apply: ● All commercial battery packs must be identical. ● Each battery pack must be independently connected to its own propulsion system and equipped to have its own arming fuse.	Propulsion	Pass
Propulsion power total stored energy cannot exceed 100 Watt-hours.	Propulsion	Pass
Maximum current rating for the arming fuse cannot exceed the maximum continuous discharge current rating of the battery pack up to 100 amps	Propulsion	Pass
Aircraft wing must be able to withstand a 2.5g load.	Structures	Pass
Empty and loaded cg locations must be marked on the exterior of the aircraft.	Structures	Pass
Aircraft radios must have a fail-safe mode where the receiver commands the following: Throttle closed, full up elevator, full right rudder, full right aileron, full flaps down.	Controls	Pass

Table 5. Mission requirements

Mission	Scoring Equation	Synopsis of Mission	Emphasized Characteristics
M1	$M1 = 1$	Crew only flight. 3 laps must be completed within 5 minutes. Takeoff within 20 feet.	Quick takeoff. Must be stable without payload. Land safely.
M2	$M2 = \frac{N(\frac{Payload\ Weight}{Time})}{Max(\frac{Payload\ Weight}{Time})}$	Payload flight (medical supply cabinet and patient). Must be 3"x3"x3.5". 3 laps must be completed within 5 minutes.	High stability with heavy payload. Land safely. Plane should fly fast.
M3	$M3 = 2 + \frac{N(\frac{\#\ of\ Laps\ *\ \#\ of\ Passengers}{Battery\ Capacity})}{Max(\frac{\#\ of\ Laps\ *\ \#\ of\ Passengers}{Battery\ Capacity})}$	Crew and passenger flight. Maximum number of laps must be completed within 5 minutes.	Quick takeoff. Plane should fly fast. Plane should be stable with different payload.
GM	$GM = \frac{Min(Mission\ Time)}{N(Mission\ Time)}$	Change between different mission configurations and the parking configuration.	Quick and easy assembly. Trained team member. Strong wings that can be configured for parking.

2.6 Mission Sensitivity Analysis

The team performed a sensitivity analysis to determine which mission specific parameters should be prioritized for optimal scoring. The analysis was split into two distinct sections. The primary parameters chosen were mission completion time versus payload weight. The team found that a focus on increasing payload weight would have a greater effect on the overall scoring values as opposed to optimizing the aircraft for speed. Analyzing the individual

variables for each scoring equation involved assessing the total payload, maximum payload, laps completed, passenger count, and battery capacity independently across all missions. Mean values for these variables were established using released specifications for comparable RC specific components [5], with mission-specific parameters determined through interior plane compartment sketches and models. The analysis underscores the significance of payload capacity as the primary design focus, evidenced by its direct correlation with weighted points. Battery capacity and passenger count were found to be less critical design variables, as the former is linked to thrust capabilities, while the latter only benefitted Mission 3. Overall payload capacity benefitted every mission. Although the number of laps completed had a notable effect, the variance is not substantial enough to warrant it as a key design consideration.

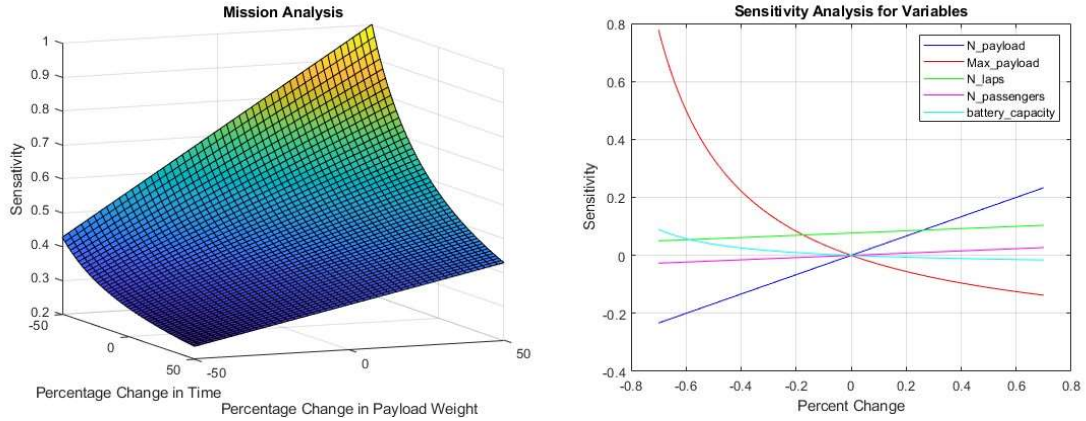

Figure 8: Sensitivity analyses visualizations.

2.7 Aircraft Configuration

The team consulted the mission requirements and reviewed decision matrices from previous DBF teams at WPI to select an optimal combination of components. Components of the aircraft were divided into the following notable sections: wing, tail, propulsion, and landing gear configurations.

2.7.1 Wing Configuration

One consideration for the main wing's position is the decision for a top-mounted, mid-mounted, or low-mounted wing. Given the team's rotating wing mounting solution for the challenge of creating a parking configuration, the top- or bottom-mounted wing configurations present themselves as leading options compared to the mid-mounted configuration. This is due to the relative ease by which a rotational mounting mechanism could be devised for a wing that is

mounted on the top or bottom of the fuselage. The decision to use a top-mounted wing versus a bottom-mounted wing was determined by compounding factors, namely comparative ease of access, enhanced ground clearance, and increased stability. A top-mounted wing's rotational mechanism is more readily accessible in the event of parking/flight configuration change than a bottom-mounted wing. A top-mounted wing also grants the team additional flexibility with regard to changing the wing's longitudinal position between design iterations that may affect its center of gravity or neutral point.

The shape chosen for the aircraft's wing was determined based on a shape's simplicity in manufacturing and its ability to support takeoff within a short distance. Furthermore, swept wings would be less efficient than other wing shapes at generating the necessary lift to takeoff within the required distance. A rectangular wing shape was chosen as a starting point for data analysis and testing due to the comparative ease in which it could be manufactured. Through this analysis and testing process it was found to be more than adequate for the needs of the mission requirements. As a result, no further adjustments to the shape of the wing needed to be made. Adding a taper to the shape of the wing had been considered initially, but it was decided that the additional manufacturing complexity outweighed potential gains in performance of the wing.

2.7.2 Tail Configuration

The tail configuration of the aircraft consists of the tail boom, horizontal and vertical stabilizers, and their associated control surfaces. Early in the conceptual planning of the plane's design, a conventional tail was selected. This was based on its ease of manufacturing as well as its efficient integration into various tail boom designs. A T-tail design would have had similar manufacturability but would have been far more difficult to attach to the tail boom. Furthermore, the team decided to adopt a tail-dragger design which necessitated the motor be mounted between the top-mounted wing and the horizontal stabilizer. A T-tail would have placed the horizontal stabilizer on the same plane as the top-mounted wing, so a conventional tail was a more sensible solution. The decision to use tail booms rather than extending the fuselage was based on the desire to reduce the additional weight's effect on the center of gravity. Dual tail booms granted the tail section more resilience against torsion than a single tail boom.

2.7.3 Propulsion Configuration

Decision categories for the propulsion systems of the aircraft were based on the placement and number of motors as well as propeller design that would be used. In the early stages of conceptual design, the decision to use a high-mounted wing would also facilitate the use of two, wing-mounted motors if such a choice was necessary. Following a theoretical analysis of the aircraft and physical testing of various motors, it was determined that a single, front-mounted motor would provide sufficient power for the plane to take-off within the required distance and maintain flight for the duration of the course. Initially, a two-motor propulsion system was considered to enhance the plane's ability to carry heavier payloads by providing additional thrust. However, this option would have added complexity in the manufacturing process and increased the plane's weight in its unloaded state. For this reason, a single mounted motor was elected as the best candidate for our propulsion system. Another consideration for the motor was the propeller configuration. Referencing tests conducted on the motor using a thrust stand, it was decided that while a three-bladed propeller would provide more peak thrust than a two-bladed propeller, it would also induce more drag and turbulent airflow. Therefore, it was decided that the extra thrust that the three-bladed propeller produced did not outweigh its negative aspects.

2.7.4 Landing Gear Configuration

The choice of landing gear for the aircraft was based largely on take-off distance and ground clearance. The use of a tail-dragger configuration would give the aircraft an advantage during take-off by having it pitch up when at a standstill. This reduces the ground roll during take-off, allowing the aircraft to become airborne within 20 feet. A lightweight, aluminum landing gear was chosen to withstand the impact of landing. The team selected 4-inch diameter wheels for the main landing gear to provide extra ground clearance.

2.7.5 Selected Configuration

The final aircraft configuration was a conventional tail, high-wing, single motor, taildragger plane. It had a rectangular wing, used a two-bladed propeller, and utilized a dual tail boom.

3 Preliminary Design

This section details the team's design methodology, the analysis performed, and expected aircraft performance.

3.1 Initial Weight Estimation

During the initial design phase, an algorithm based on historical data was created to estimate the total weight of the aircraft. This was broken down into crew, payload, battery, and empty weight. The individual weights were added together to obtain the gross weight of the aircraft for the specified

missions

$$W_{total} = W_{crew} + W_{payload} + W_{battery} + W_{empty} \tag{3.1}$$

The crew and payload weights were determined by measuring the respective weights of the wooden peg dolls. The battery and empty weight were unknown values that were calculated as a function of the total weight of the aircraft using Equation 3.2. These values are represented as BMF and W_{empty}/W_{total}. The algorithm iteratively calculated the battery mass fraction and the empty weight ratio for each mission leg during flight. Figure 9 provides a summary of how the algorithm iteratively calculated the total weight of the aircraft.

$$W_{total} = \frac{W_{crew} + W_{payload}}{1 - BMF - \frac{W_{empty}}{W_{total}}} \tag{3.2}$$

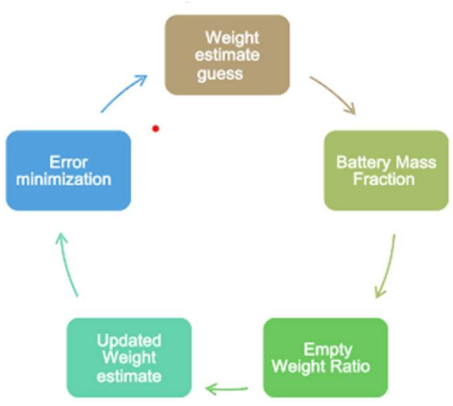

Figure 9: Weight estimation analysis loop.

Table 6 provides a summary of the calculated battery mass fraction (BMF) and corresponding formulas used for each mission segment.

Table 6: Battery mass fraction calculation for each mission leg

Mission Segment	Formula	BMF
Take-off	-	0
Climb	$\frac{T_{climb} * P_{motor} * 1000}{3.6 * E_{sb} * n_b} * W_{total}$	0.0481
Cruise	$\frac{R * g}{E_{sb} * n_b * n_p}$	0.0454
Land	-	0.0985

The values obtained for the battery mass fraction were important in the power consumption estimation for each mission. With these initial estimates, a refined analysis was performed to determine the number of batteries needed for the completion of all missions. Using Equation 3.2 and parameters detailed in Table 6, an initial weight estimate of 8.80 pounds was obtained. This measurement represented the maximum allowable weight of the aircraft.

3.2 Aerodynamic Analysis

The aerodynamic analysis was approached with a focus on cruise velocity, weight of the aircraft, and the desired flight altitude. These parameters allowed for the calculation of the required lift coefficient and corresponding Reynolds number. The Reynolds number for the aircraft was based upon a projected flight speed of 60 ft/s, a chord length of 1 foot, and standard atmospheric conditions at sea-level, and it was calculated using Equation 3.3. This parameter was useful in describing the expected flow profile over the aircraft. Since the expected flight speed of the aircraft was relatively low, the calculated Reynolds number was in the order of 1 hundred. This indicated that the aircraft would be experiencing significant viscous forces.

$$Re = \frac{\rho V c}{\mu} \tag{3.3}$$

Using the initial weight estimate of 8.80 pounds, projected flight speed, air density, and physical wing characteristics such as span and chord length, the coefficient of lift required for the aircraft was calculated using Equation 3.4. The coefficient of lift was a dimensionless parameter that was used to describe the ability of the aircraft to produce lift. In this calculation, the $C_{L_{required}}$ represented the minimum C_L required for the aircraft to maintain flight.

$$C_{L_{required}} = \frac{W}{\frac{1}{2}\rho V^2 S} \tag{3.4}$$

From the calculated Reynolds number and C_L, XFLR5 software was utilized to find suitable airfoils that match the design specifications. Table 7 provides a summary of key parameters calculated in this section.

Table 7: Key parameters

Parameter	Value
V	$60\ \frac{\text{ft}}{s}$
ρ	$0.0024 \frac{\text{slug}}{\text{ft}^3}$
c	1 ft
μ	$3.78445 * 10^{-7} \frac{lb - s}{\text{ft}^2}$
Re	380000
$C_{L_{required}}$	0.3896

3.2.1 Airfoil Selection

Airfoil analysis and subsequent selection was performed on NACA airfoils, as they are well-documented and researched. This made the analysis and manipulation of various airfoils in XLFR5 simpler. Due to the limited take-off distance, it was imperative to choose a high lift airfoil to meet that requirement. To achieve the required lift coefficient of 0.3896, a cruise angle of attack of 3º was selected.

The following airfoils met this requirement: NACA 4412, NACA 4416, NACA 2412, NACA 6409. To further narrow the airfoil selection, the focus of the analysis shifted to the

behavior of each airfoil's stall characteristics. This allowed the team to ensure desirable lift characteristics were present throughout the entire flight envelope, including at stall conditions. The graphs produced from XFLR5 are displayed in Figure 10.

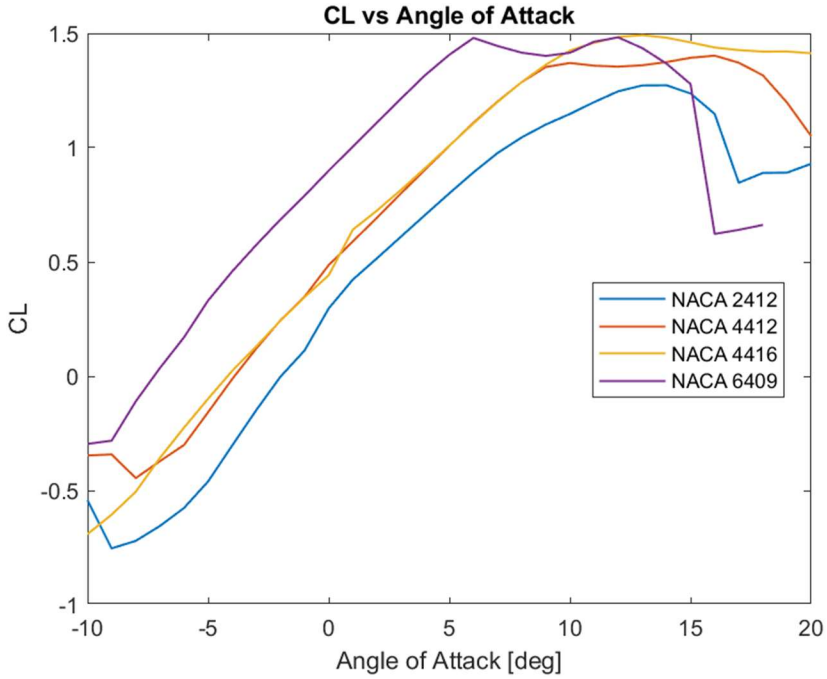

Figure 10: Plot of CL vs AOA for selected airfoils.

As shown in Figure 10, the NACA 2412 airfoil was not chosen for our aircraft because it produced the least amount of lift throughout the chosen AOA. The NACA 6409 was not selected due to its very low stall angle of attack. This airfoil had too much camber for the aircraft's low airspeed. The NACA 4416 had a similar lift profile to the NACA 4412. However, as a result of its greater thickness, the NACA 4416 generated 0.037 lbf more drag than the NACA 4412. As a result, it was determined that the NACA 4412 had a desirable combination of both lift profile as well as drag minimization. The stall velocity of 15 ft/s was calculated for the defined flight envelope using Equation 3.5.

$$V_{stall} = \sqrt{\frac{2W}{\rho CL_{max} S}} \tag{3.5}$$

The airfoil analysis was further extended by validating the theoretical results with experimental results from a wind tunnel. This experimental data presented in Figure 11 shows a lift profile that was expectedly lower than the theoretical results. This was a result of the flow separating from the airfoil, producing less total lift. This trend of experimental data being lower than theoretical data was followed in all practical tests.

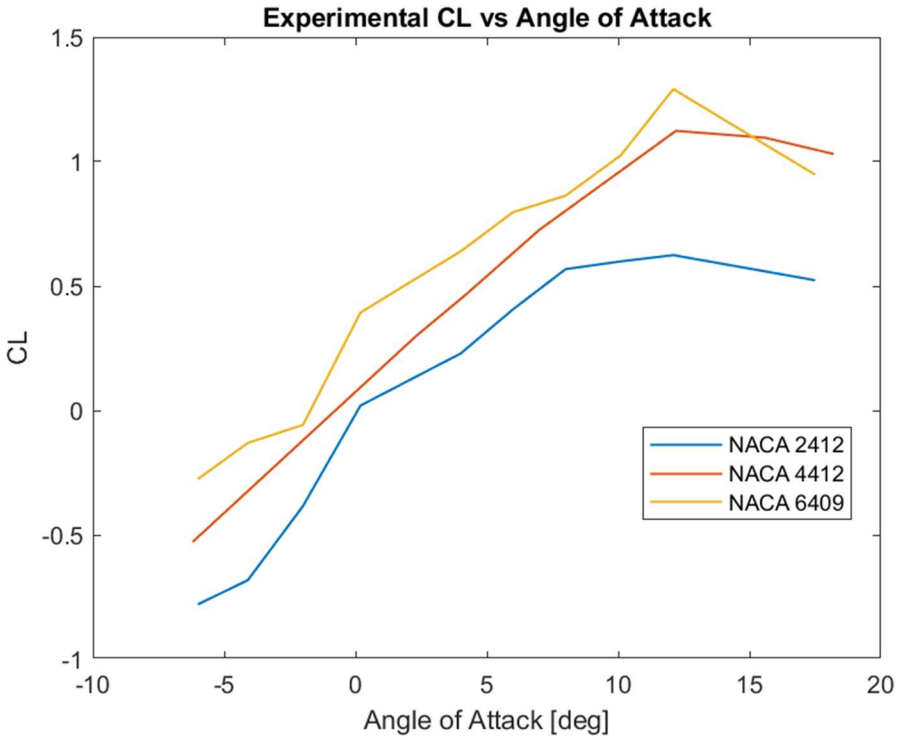

Figure 11: Experimental CL vs AOA for selected airfoils.

3.2.2 Wing Sizing and Geometry

3-D models of the aircraft's aerodynamic bodies were created using XFLR5 for the purpose of analyzing different wing and tail configurations. Figure 12 depicts the final configuration of the wing and tail segments. The wing design featured a rectangular shape, which helped to maintain a constant Reynolds number across the wingspan.

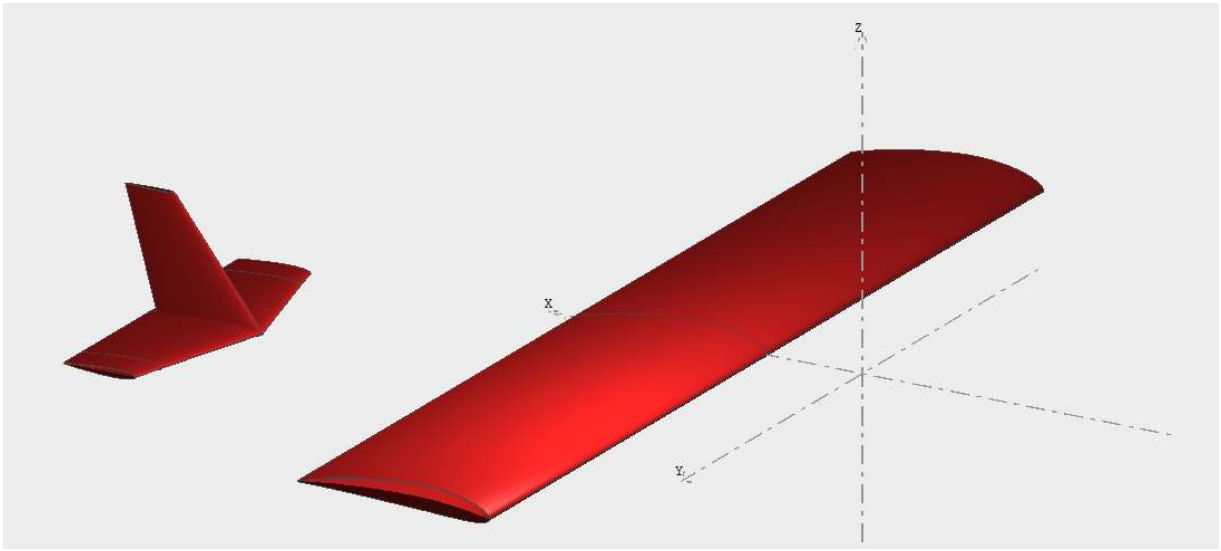

Figure 12: Wing and tail configuration.

XFLR5's 3-D analysis tool was used to predict the aircraft's performance. Due to the limitations of the available wind tunnel in terms of velocity, the simulations were run at a constant cruise speed of 98 ft/s over a varying angle of attack from -5 to 20 degrees. The operating conditions for the wind tunnel were calculated using dynamic similarity. The calculated values for the coefficients of lift, drag, and moment are shown in Table 8. The negative value obtained for the moment coefficient, C_M, indicated that at cruise, the aircraft would experience a nose-down pitching moment, reducing the angle of attack of the aircraft without control input.

Table 8: Aerodynamic coefficients at cruise conditions

Aerodynamic Coefficients	Value
C_l	0.581
C_d	0.0347
C_m	-0.250

To validate the theoretical analysis, a scale wing model was created using additive manufacturing for wind tunnel testing. A picture of the 3D printed wing model is presented in Figure 13. Because of the constraints in the capabilities of the wind tunnel, the team was not able to conduct tests on the wing and tail sections together. As a result, it was assumed that the impact on lift and drag characteristics from the tail section were small in comparison to the contribution by the wing.

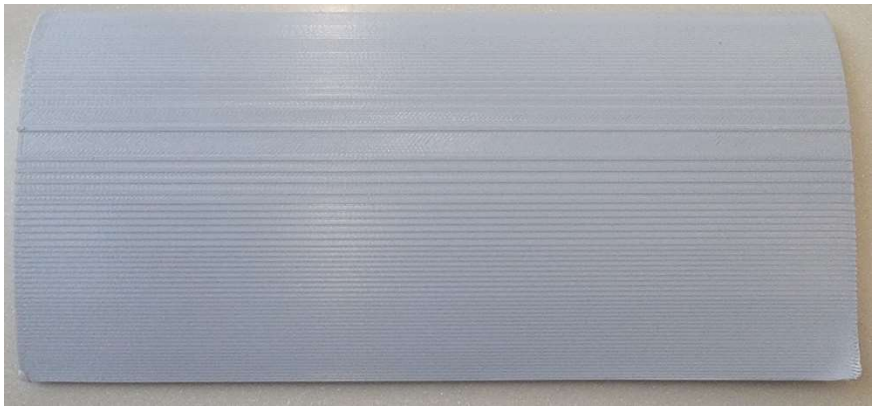

Figure 13: 3D printed scaled wing model.

Figure 14 is a plot of the coefficient of lift vs angle of attack. The experimental C_L values were calculated using Equation 3.6 which relates the normal and axial forces evaluated at the angle of attack measured during the wind tunnel testing and Equation 3.7 which provides the formula used to find the coefficient of lift given the lift force, air density, flight speed and wing area. The plots of the experimental C_l and the theoretical C_l exhibited a similar trend, which validated the theoretical results.

$$L = Ncos(\alpha) + Asin(\alpha) \tag{3.6}$$

$$C_L = \frac{L}{\frac{1}{2}\rho V^2 S} \tag{3.7}$$

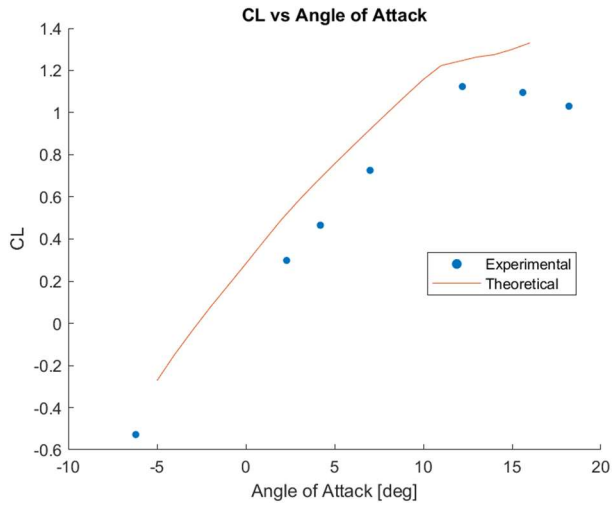

Figure 14: Plot of the coefficient of lift vs angle of attack.

Figure 15 is a plot of the C_m vs angle of attack with respect to the quarter chord point. Equation 3.8 and 3.9 provides the formulas used in the calculation for the $Cm_{c/4}$. The sensor used to measure the pitching moment in the wind tunnel was not aligned with the quarter chord point on the airfoil. Therefore, to calculate $M_{c/4}$, the pitching moment, M was subtracted from the moment arm (c*N) where c represented the offset distance and N represented the normal force. The trend in the plots depicted by the experimental and theoretical data is characterized by a negative slope. This indicated that the aircraft had positive stability because as the angle of attack increases, the C_m decreases.

$$M_{\frac{c}{4}} = M - (c * N) \tag{3.8}$$

$$C_{M_{\frac{c}{4}}} = \frac{M_{\frac{c}{4}}}{\frac{1}{2}\rho V^2 Sc} \tag{3.9}$$

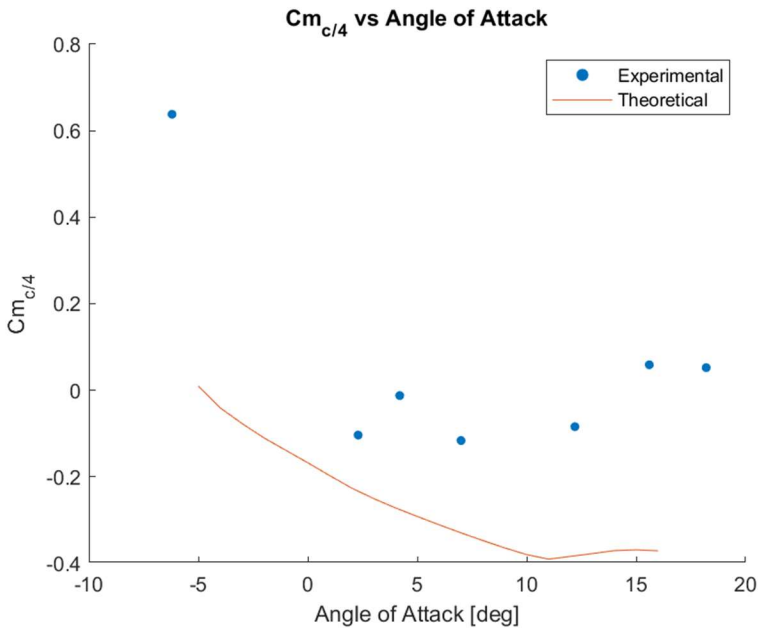

Figure 15: Plot of $C_{m,c/4}$ vs angle of attack.

3.2.3 Tail Analysis

The team decided that the horizontal tail should be a 1/4-inch-thick flat plate. This is best analyzed using finite wing theory, where airflow is modeled around a wing of finite span. Using the Kutta-Joukowski theorem [6], it is known that for two dimensional, inviscid, incompressible flow around a closed contour, the lift per unit span is proportional to the circulation strength around the body and the freestream velocity. This is typically expressed as: $L = \rho \Gamma V_\infty$, where ρ is the fluid density of air, Γ is the circulation strength, and V_∞ is the freestream velocity. For a flat plate airfoil, the circulation strength can be calculated knowing that there is no net circulation around the airfoil in inviscid flow. The flow around a flat plate results in a trailing vortex. The circulation strength is constant along the airfoil's span and is equal to the strength of the starting vortex.

As a result of viscosity and flow separation, the airflow cannot smoothly interact with the sharp trailing edge or flow around it without encountering any disturbances. The freestream separates from the airfoil leading to something known as the Kutta condition. There is a specific value of the circulation strength, that of $\Gamma = V_\infty c\pi\sin(\alpha)$, where c is the plate's chord length, that causes the flow to leave the trailing edge smoothly. Using this value for circulation strength it can be determined:

$$L = V_\infty c\pi\sin(\alpha)\,\rho V_\infty = \rho V_\infty^2 c\pi\sin(\alpha) \tag{3.10}$$

$$C_l = \frac{C_L}{b} = \frac{2L}{\rho V_\infty^2 c} = \frac{2\rho V_\infty^2 c\pi\sin(\alpha)}{\rho V_\infty^2 c} \tag{3.11}$$

$$\& \text{ using } \sin(\alpha) \approx \alpha$$

Therefore, it can be estimated that for the plane's flat plate tail section, the coefficient of lift per unit span is $C_l = 2\pi\alpha$ where α is the angle of attack of the tail. Using these results, the coefficient of lift can be found at any angle of attack. In practice, these assumptions held true for angles up to about 12°.

3.2.4 Lift and Drag Analysis

To better understand the amount of drag produced, an in-depth analysis was performed on every external component of the aircraft. This was particularly important as the data would provide a good estimate of the power required to counteract drag effects during flight. The total drag of the aircraft was calculated by taking the sum of the parasitic drag, induced drag, and pressure drag. Equation 3.12 shows the formula used in the calculation for the total drag. The parasitic drag, represented by C_{D_0} in the equation, was estimated as 0.03 using historical data from Raymer's text [2]. An aspect ratio of 5 and Oswald efficiency factor of 0.7 were calculated for the analysis. The total drag produced was calculated for different flight velocities to have data that would describe the performance of the aircraft from stall to take-off conditions. This involved calculating the C_L of the total aircraft. Equation 3.13 provides details of the formula used.

$$C_D = C_{D_0} + \frac{C_L^2}{\pi ARe} \tag{3.12}$$

$$C_L = \frac{W_c}{\frac{1}{2\rho V_c^2 S}} \tag{3.13}$$

The calculated drag measurements at various velocities were compared to thrust output measurements from the motor. The plot shown below displayed the drag and thrust as a function of velocity. The point at which the two curves intersect provided information about the optimal cruise and take-off conditions. Figure 16 depicts that the designed cruise velocity of 60 ft/s is less than the velocity from the thrust drag plot. These results show that the motor will be underpowered during missions, allowing the aircraft to achieve higher speeds with less power.

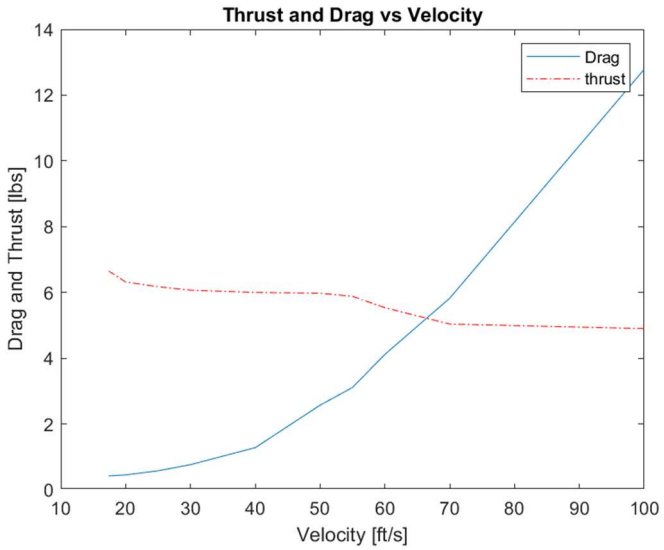

Figure 16: Plot of drag and thrust as functions of flight velocity.

With the measurement of the total drag, further analysis was performed to find the required thrust and power for flight. The power required was found by taking the total drag multiplied by the cruise velocity. To refine the velocity measurement, the power produced was calculated for a range of velocities between the stall and 1.2 times the desired cruise velocity. A plot of the power required and total drag versus velocity was generated to analyze the effects on thrust and drag as the velocity of the aircraft increased. As depicted in Figure 17, increasing the flight velocity leads to an increase in the power required to overcome drag effects. This plot helps with power output optimization for a given velocity.

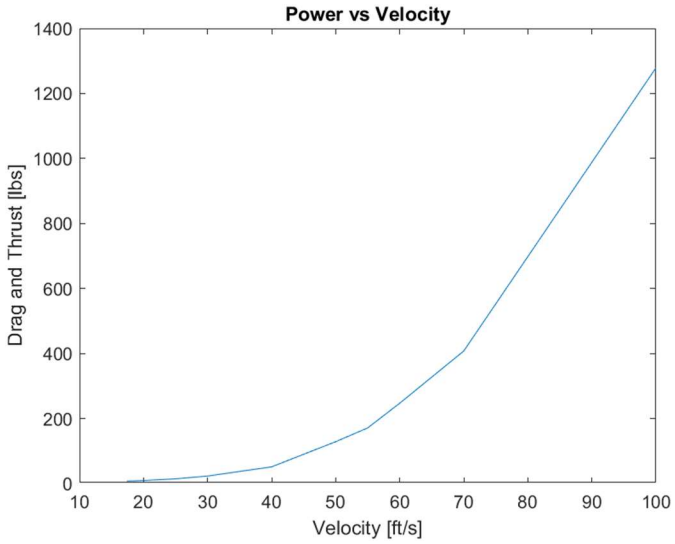

Figure 17: Plot of power required vs flight velocity.

3.2.5 Pitch Analysis

XLFR5s plane analysis was utilized to simulate the airflow and pressure distribution across the wing. Performing this analysis over a range of angle of attack values and combining the results of these individual tests enables an animation of the pressure distribution and flow changes to be created, allowing the team to anticipate conditions that the aircraft will experience as it pitches up and down during flight.

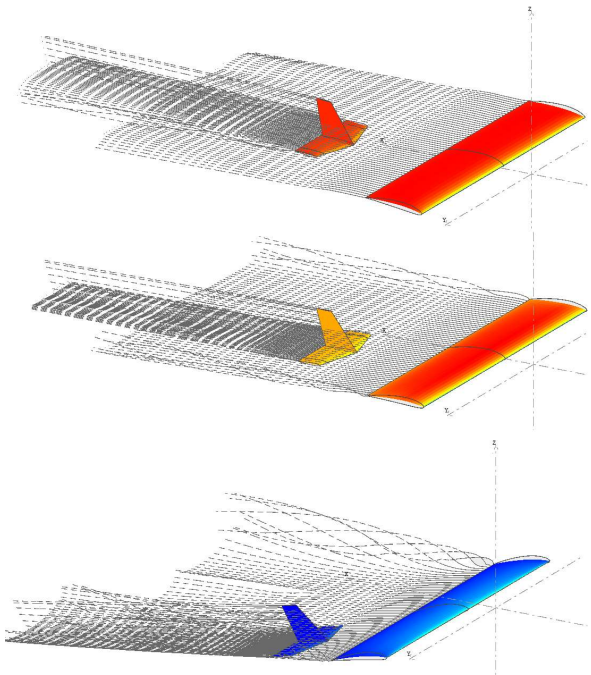

Figure 18: Pressure distribution and flow for aircraft at -5° (top) 0° (middle) and 13° (bottom).

From this analysis there are several key takeaways that can help to understand the flight characteristics of the aircraft. Firstly, at extreme angles of attack, there is an area of lower pressure across the leading edge of the aircraft wing. This shows that the leading edge is dominating the lift generation of the aircraft in high angle of attack positions. There is also minor flow separation near the tail section during negative angles of attack. In level flight, the area with a pressure differential moves to the quarter chord of the aircraft wing. The wing tip vortices pull a significant amount of the air away from the centerline of the aircraft. Vortices of this size may produce a significant amount of induced drag. This can lead to a reduction in the lifting capabilities of the wing, causing a decrease in the plane's ability to take-off within 20 ft.

3.2.6 Take-off Distance

The competition this year imposed a take-off distance of 20 feet. The aircraft design process prioritized the ability to generate significant lift at relatively lower velocities, ensuring compatibility with the motor and battery discharge capabilities. A take-off velocity of 50 ft/s was estimated for this analysis where the corresponding coefficient of lift and drag were evaluated utilizing XFLR5. The maximum value of lift occurred at 12 degrees angle of attack; however, a safety factor was incorporated to avoid operation under stall conditions. As a result, an angle of attack of 10 degrees was selected, corresponding to a lift coefficient of 1.16 and drag coefficient of 0.105. With this information, the take-off distance was calculated using Equations 3.10 and 3.11. At the determined maximum conditions, the lift generated was calculated to be 14-pound force and the corresponding drag was calculated to 1.27-pound force. As presented in the initial weight analysis, the weight of the aircraft was found to be 8.80 pounds. Utilizing the equations shown below, the predicted take-off distance was estimated to be 18.35 feet. Figure 19 depicts the dynamical problem that was solved to find the take-off distance.

$$\alpha_{ground\ roll} = \frac{32.2}{W}\big((T - D) - 0.015(W - L)\big) \tag{3.14}$$

$$S_{ground\ roll} = \frac{V^2}{2 * \alpha_{ground\ roll}} \tag{3.15}$$

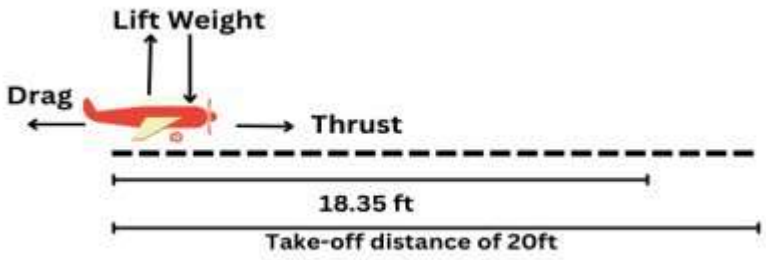

Figure 19: Take-off distance analysis.

The estimated take-off distance meets the 20 feet requirement. It is essential to note that this occurs at maximum discharge from the propulsion system. Battery charge longevity will need to be assessed to estimate battery life during missions.

3.3 Controls Analysis

3.3.1 Static Stability Analysis

The neutral point is a critical component when analyzing an aircraft's static stability. When designing the aircraft, it was important that the neutral point fell in a location behind the center of gravity to ensure static stability. Another important consideration is the static margin; as the distance between the CG and the neutral point increased, the effect the control surfaces have on the aircraft's attitude decreased.

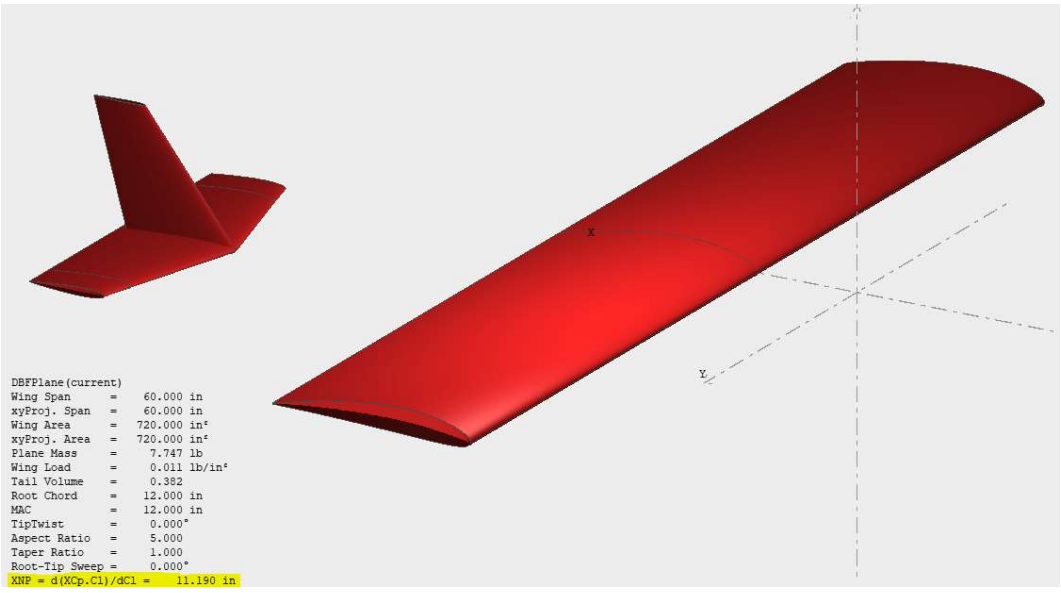

Figure 20: XFLR5 neutral point analysis.

Using the model developed in Section 3.2.2, the team calculated the aircrafts neutral point using the XFLR5's 3D analysis tool. The location of the neutral point was found to be 11.19 inches from the front of the fuselage. Based on historical data, this value made sense.

The static stability of the aircraft can be described by the position of the neutral point relative to the position of the center of gravity. To find the location of the center of gravity, the weights of individual aircraft components were measured. These weights were then added into the 3-D model as point masses in their relative positions. Running this new analysis, the team was able to calculate the location of the center of gravity and compare it with the neutral point.

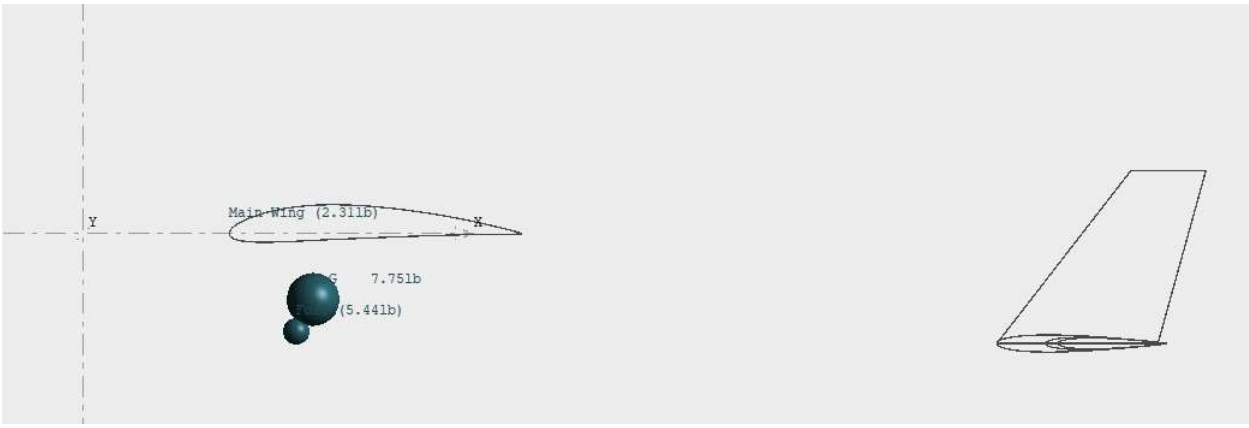

Figure 21: Mass locations relative to wing and tail.

From the analysis, the center of gravity is 9.438 inches from the nose of the aircraft while the neutral point is 11.19 inches from the nose of the aircraft. Using Equation 3.16, a static margin of 14.6% of the aircraft's mean aerodynamic chord is calculated. The neutral point's position behind the center of gravity ensures that the plane is statically stable. This behavior ensures ease of maneuverability and aircraft responsiveness. The locations of the center of gravity as well as the neutral point are shown in Figure 22.

$$SM = \frac{X_{NP} - X_{CG}}{MAC} \tag{3.16}$$

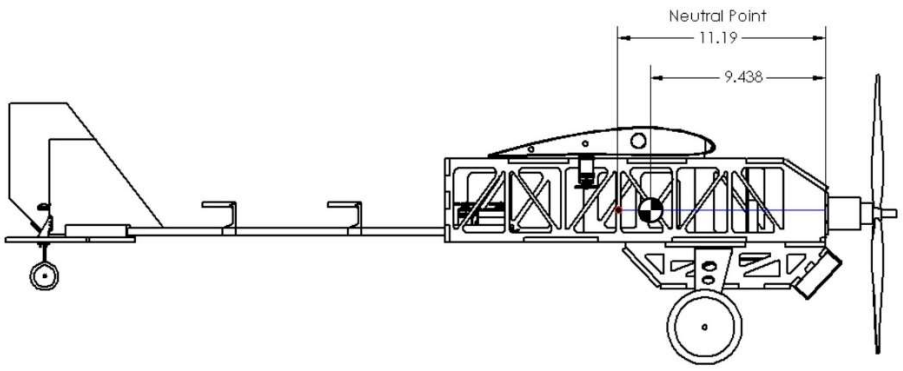

Figure 22: Location of center of gravity and neutral point for non-payload flight.

3.3.2 Control Surface Sizing

For the preliminary design of control surface sizing, the team utilized an approach drawn from Andy Lennon's textbook, *The Basics of RC Model Aircraft Design* [3]. The sizing of the control surfaces followed Lennon's fundamental guideline of basing the area of the surfaces as percentages of wing or tail area. Specifically, the area of the ailerons were designed at 35% of the wing's span, and 25% of the wing's chord. The area of the flaps were designed to at 65% of the wing's span, and 20% of the wing's chord. These relations can be found in Figure 23.

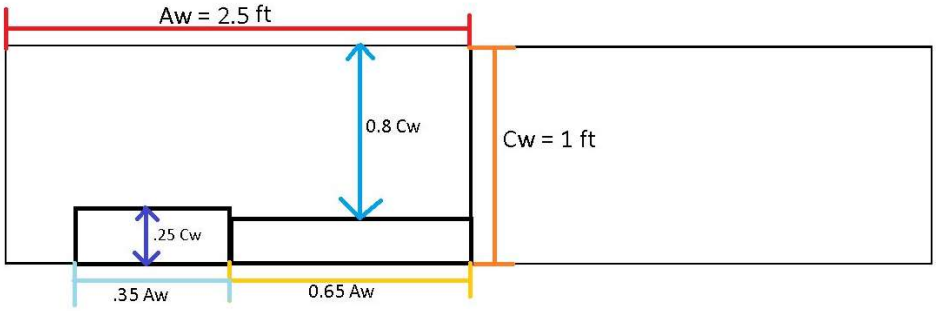

Figure 23: Control surface sizing of the main wing.

This approach allowed the team to quickly adjust sizing with different iterations. With any change in the wing sizing, the control surface area would be adjusted accordingly, in order to meet the evolving needs of the design.

The same approach applied to the control surfaces of the horizontal and vertical tail. The preliminary design consisted of an elevator that has a span of 8% of the main wing's span and chord length of 6% of the main wing's span. The rudder had a span of 4% of the main wingspan, and a chord length of 10.5% of the main wing's chord. It is important to note that these ratios and sizings were eventually updated to those of Section 4.3.1 and 4.3.2.

For the preliminary design of control surface sizing, the team based the sizing of the control surfaces off the outline of the Sw.

3.3.4 Trim Analysis

In a typical tail dragger configuration, standard trim models include zeroing the incidence of the horizontal stabilizer, then setting the incidence of the main wing and motor relative to that. Trimming an aircraft is very useful in keeping it on its intended flight path in a predictable and efficient manner by relieving pressure off the control surfaces. With properly applied trim conditions, there is minimal input required from the pilot to maintain level flight. Initially, a standard setup was used, with the horizontal stabilizer set to 0°, main wing set to 2°, and the motor set to 0°. After flight tests at this configuration, there were stability issues with the plane. This required a reassessment of the trim configuration. The motor was adjusted to an angle of -2°, however, after flight testing, it was determined that this adjustment was too aggressive. The instability of the plane increased with this change. The motor was then mounted at -0.5°. Flight testing this configuration led to drastic performance increases, even allowing the plane to be put through performance maneuvers like rolls, loops, and accelerated stalls.

3.4 Propulsion Analysis

3.4.1 Battery Analysis

Initial battery design discussions involved decisions between 4 cell and 5 cell batteries. It was decided to test the performance of both batteries using the RCbenchmark static thrust stand. Without changing the propeller configuration max thrust and power draw tests were completed using both a 4 cell and 5 cell battery. After the test the 4-cell layout produced a peak thrust of 8.04 pounds and a maximum draw of 847 Watts at 55 amps. The 5-cell layout produced a peak thrust of 10.67 pounds and a maximum draw of 1252 Watts at 70 amps. Considering the short take off distance, the 32.7114% increase in thrust from the 5-cell battery was chosen. Further analysis on the battery was used to determine total endurance of the aircraft. At maximum thrust, aircraft endurance is 4 minutes 23 seconds, at half throttle endurance in 8 minutes 57 seconds, and under mixed throttle endurance is 11 minutes 7 seconds. The mixed throttle test simulates

most closely the experience during mission flight and should provide more than enough time for all mission completion.

3.4.2 Motor and Propeller Sizing

Motor and propeller sizing began with what was available to the team left over from previous years. After analyzing the budget of the previous year's team, it was found that they spent around 30% of their budget on the motor; therefore, using a motor already available to the team would save a significant amount of money. Of the initial four motors that the team was left with, two could be removed immediately due to weight and power. The motors that were left were the Scorpion SII-4020-540Kv and the Scorpion HK-3226-900Kv, of which the SII-4020-540Kv seemed to produce more thrust based on a theoretical test using MotoCalc8, shown in Figure 24. After the theoretical test, the motor along with two propellers and two batteries were tested on the RCbenchmark static thrust stand, seen in Table 9. The test was done to see which combination would yield the highest peak thrust, which was found to be the 15-6 propeller and 5 cell battery.

Table 9: Peak thrust for varying propulsion setups

Propeller and Battery Combination	Peak Thrust
15-6 and 5 Cell Battery	10.67 lb/ft
14-6-10 and 5 Cell Battery	10.15 lb/ft
14-6-10 and 4 Cell Battery	8.04 lb/ft
15-6 and 4 Cell Battery	7.91 lb/ft

Table 10: Motor specifications and power output

Motor	Weight	Kv Rating	Max Continuous Power	Max Continuous Current
Scorpion SII-4020-540Kv	288 g	540 RPM/V	1850 Watts	85 amps
Scorpion HK-3226-900Kv	239 g	900 RPM/V	1770 Watts	60 amps
AXI 4130-20	409 g	305 RPM/V	N/A	55 amps
A40-12L 14 Pole	272 g	410 RPM/V	1100 Watts	N/A

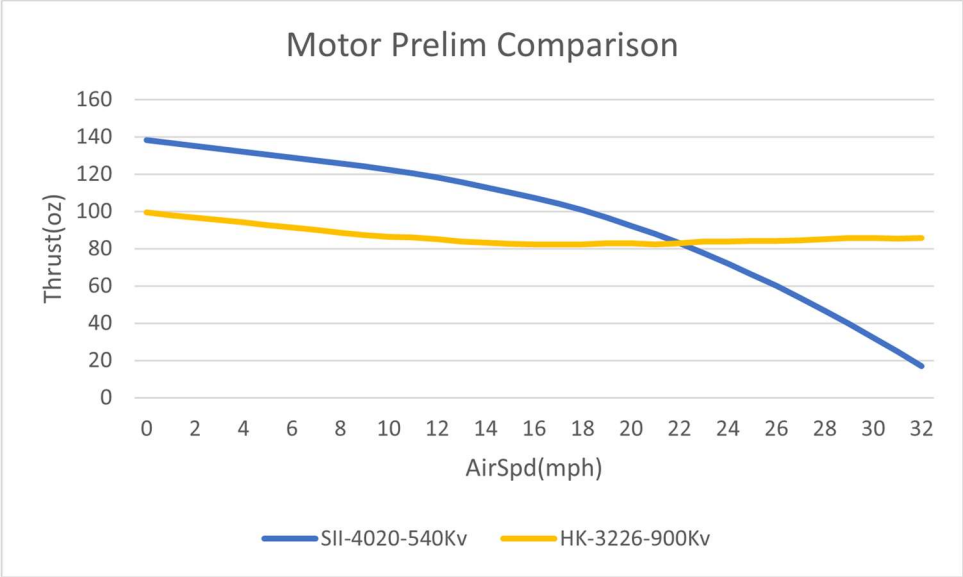

Figure 24: Plot of theoretical thrust velocity for two motors.

3.5 Structural Analysis

To create the preliminary design of the aircraft, multiple design iterations were completed: first through sketches, then CAD modeling, and then finally through numerical modeling within the ANSYS software. The team wanted to create the lightest possible aircraft design that maximizes mission payload. Additionally, the team wanted to emphasize strength within the design and minimize failure points, especially along the wing.

Analysis was heavily focused on contact points within the wing, the wing to the fuselage, the fuselage components, and the fuselage to the tail control surfaces.

3.5.1 Fuselage Sizing and Design

The fuselage sizing was based on the payload requirements and additional competition restrictions. In terms of height, the absolute minimum height required was based on the height of the passenger, which was 3.5 inches. Additional height was added to ensure the team was able to access the interior as well as space for any mission inserts. In terms of width, the absolute minimum required was based on the medical supply cabinet and the width of 2 crew, which was 3 inches. Additional length was added to ensure clearance with the walls of the fuselage. In terms of length, the absolute minimum was based around the Mission 2 payload requirements, which was 10 inches. Additional length was added for the receiver battery, clearance with the walls of the fuselage, and clearance between each payload.

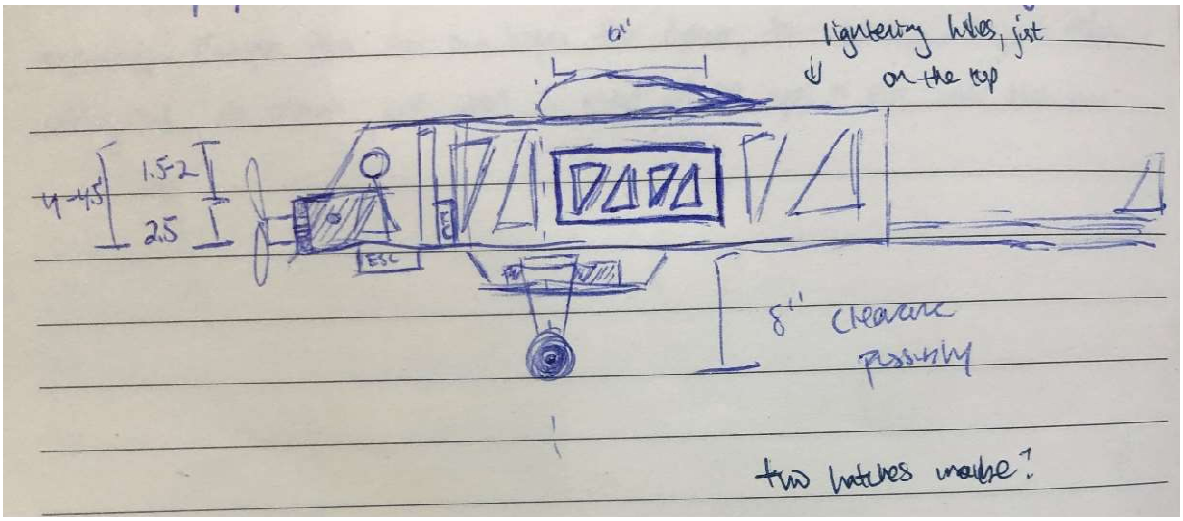

Figure 25: Sketch of fuselage.

The shape of the fuselage was dependent on 2 factors: ease of manufacturing and its aerodynamic properties. Possible shapes discussed were airfoil, circular, and rectangular. The team decided to make the fuselage rectangular, as the ease of manufacturing outweighed any benefits from other shapes. A rectangular fuselage also allowed for a simpler wing attachment and rotational mechanism.

3.5.2 Wing Deflection Analysis

As the team advanced into the design process, the loads experienced by the wing were analyzed. This process involved sizing the main wing spar and selecting an appropriate material that could withstand the expected wing loading.

In the design of the wing spar, carbon fiber was selected due to its high strength and low weight properties. This was suitable for the design of the aircraft as the team sought a low weight material that offered high strength properties, thereby allowing us to increase load carrying capacity for missions. A circular cross-section was selected for the shape of the wing spar due to its strength, stiffness and ease of manufacturability. It also allows for the uniform distribution of applied loads throughout the span thereby making the wing resistant to bending forces. Additionally, the stiffness provided by a circular wing spar was crucial in protecting the wing against torsional forces and maintaining the structural integrity of the wing during flight. Lastly, circular cross-section spars are relatively easy to manufacture which reduced the production cost and manufacturing time. The dimensions of the spar included an inner diameter of 0.70 inches

and an outer diameter of 0.77 inches. The chosen airfoil, NACA 4412 determined the dimensions of the wing spar. With a maximum thickness of 12 % of the chord length, totaling 1.44 inches, the dimensions of the spar were sized appropriately to ensure that it remained within the maximum thickness limit. Equation 3.17 was used to calculate the moment of inertia where do and di in the equation represented the outer and inner diameter respectively. The moment of inertia was calculated to be 0.1354 in^2. A shear modulus of 1305.34 KSI was taken from the ANSYS Material Library for the carbon fiber tube.

$$I = \frac{1}{2}\left(\frac{d_0^2}{2} - \frac{d_i^2}{2}\right) \tag{3.17}$$

To ensure that the carbon fiber spar would be sufficient to hold the weight of the plane, a preliminary cantilever beam analysis was performed to test the deflection of the spar under maximum loading conditions by evaluating the bending moment, and shear stress along its length. Since the spar remained fixed at the fuselage of the plane, analysis was simplified to that of a pinned cantilever beam. Symmetry in the load distribution was assumed where analysis was performed on half of the wing. A rectangular lift distribution profile was selected for the analysis of forces and moments. Figure 26 illustrates the lift distribution. The maximum load limit of 8lbs was evaluated by halving the weight of the plane multiplied by load factor of 2. The structural analysis of the wing spar was performed using MATLAB software.

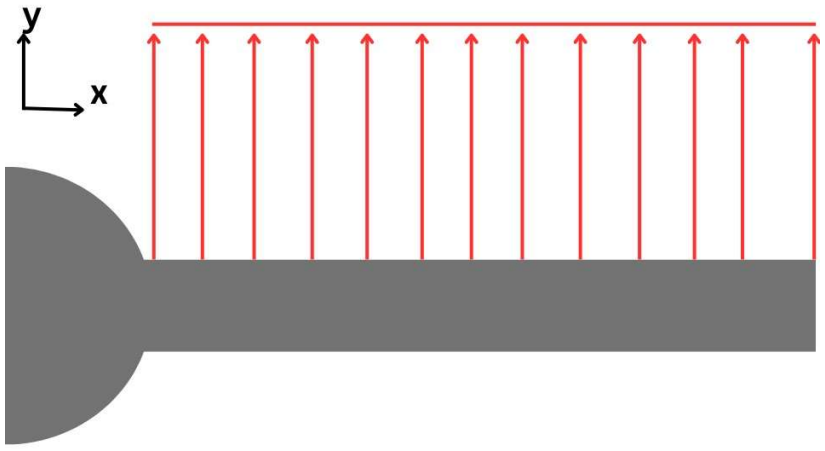

Figure 26: Rectangular lift distribution along the wing spar.

To find the bending moment and shear stress variation, the analysis was reduced to small sections along the wing spar where the parameters were evaluated at each segment. Equation

3.18 provides details on the formula used to calculate the bending moments. In the equation, w represents the uniform load acting on the span, L represents the span length and x represents the small segments along the span at which the moment and shear forces were evaluated at.

$$M(x) = \left(\frac{w}{2}\right) * (L^2 - x^2) \tag{3.18}$$

Using Equation 3.18, the following plot was generated for the bending moment.

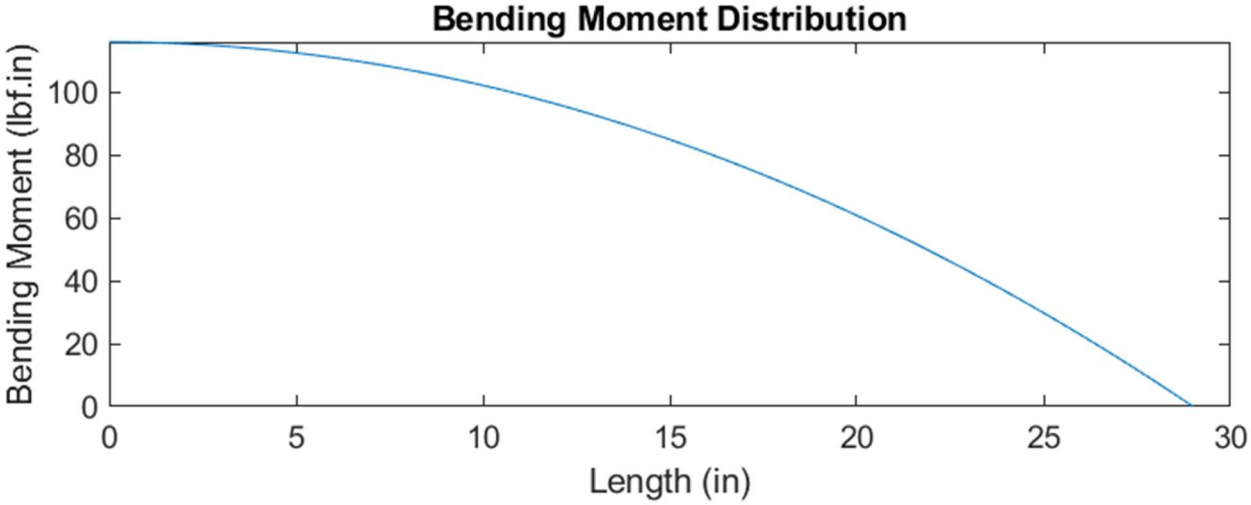

Figure 27: Bending moment vs length of beam.

The graph shows the results of the bending moment being a maximum at the root of the wing, and a minimum at the tip of the wing. The trend shown in the plot accurately describes how the moment would vary along the wingspan during flight.

Using the variation of moment, the deflection of the beam was evaluated. This involved analyzing the amount of deflection at the tip of the wing due to bending moments that acted along the wingspan. Equation 3.19 describes the formula used to find the deflection of the spar. The bending moment, M(x), is the second derivative of deflection with respect to the position along the spar. E is the modulus of elasticity, and I is the moment of Inertia of the carbon fiber spar.

$$\frac{d^2w}{dz^2} = \frac{M(z)}{EI_{xx}} \tag{3.19}$$

By integrating twice, Equation 3.20 was derived as the formula for the maximum deflection.

$$\delta_{max} = (w * l^4)/(8 * E * I) \tag{3.20}$$

The predicted maximum deflection was 0.138 inches. 0.138 inches falls within the acceptable range of deflection. For structural integrity it was required that the total deflection of the spar should not exceed 10% of its total length. In this case, the deflection was 0.48% of the length of the beam which was within the acceptable range. It was important to maintain a small wing tip deflection to reduce the risk of deformation of the wing during flight. This was because large deformations can lead to drastic changes to the flight characteristics of the plane. If not properly addressed, it could lead to catastrophic structural failure. The design of our wing features wooden parts that would be susceptible to deformation under load. Therefore, selecting a suitable wood that offered a high strength was a primary concern that was addressed during manufacturing.

The next result from the analysis was the variation shear stress along the spar. Equation 3.21 was used for this calculation.

$$V(x) = -w * (L - x) \tag{3.21}$$

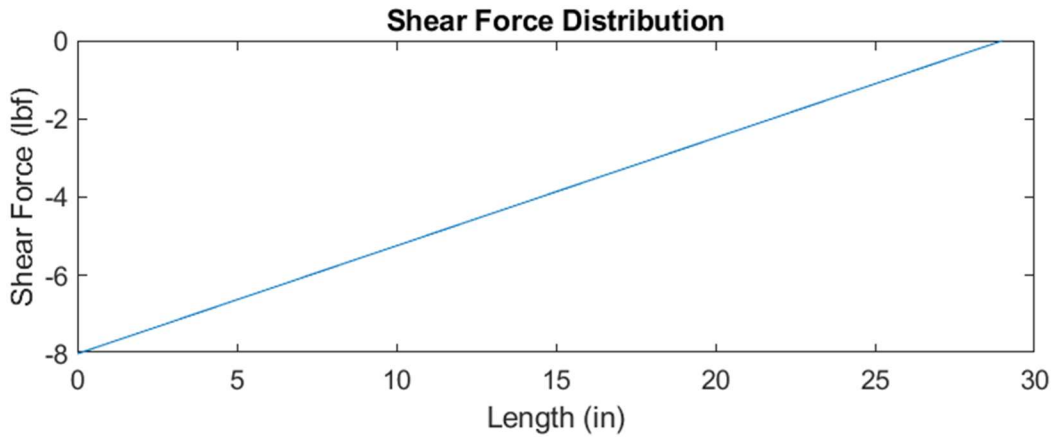

Figure 28: Shear force vs length of beam.

The shear force was acting in the negative direction where it had a negative maximum value at the root of the wing and increased to zero along the span. The maximum shear stress of the spar was also evaluated using Equation 3.22 and was found to be 26.3 PSI. Although there was no standard value for ultimate shear strength, it is common practice to estimate this value as 60% of the ultimate tensile strength. The ultimate tensile strength of carbon fiber was estimated to be 500 KSI. This gave ultimate shear strength of 300 KSI. The shear stress was significantly lower

than the ultimate shear strength of the spar. Therefore, it was concluded that the spar was safe to use under the described loading conditions.

$$\tau = V * Q/(I * t) \tag{3.22}$$

There are a few shortcomings of this type of analysis. The analysis assumes that the carbon fiber spar will take all the bending and shear stresses. Many of the other pieces in the wing design are to help the wing maintain its shape under load, and to prevent torsion of the wing. These shortcomings are covered in ANSYS analysis that was performed that used a CAD model of the wing, rather than just the carbon fiber spar.

4 Detailed Design

4.1 Dimensional Parameters

Table 11: Design Parameters table.

Wing		Horizontal Stabilizer		Propulsion	
Airfoil	NACA 4412	Airfoil	NACA 0011	Motor Model	Scorpion SII-4020-540Kv
Span	58.75 in	Span	19.00 in	Motor Rated KV	540
MAC	3in	Chord	6.99 in	Motor Weight	288 g
AR	5	AR	2.72	Propellers	15-6 in
Area	713.813 in^2	Area	109 in^2	Propulsion Battery	Liperior 5000mAh 5S 60C 18.5V
Root Chord	12.15 in	Angle of Incidence	2˚	Propulsion Battery Capacity	5000mAh
Tip Chord	12.15 in	Fuselage		Max Discharge Rate	5 C
Taper Ratio	0	Total Length	16 in	Weight	815 g
Leading Edge Sweep	0	Nose Length	4.3 in	ESC	
Angle of Incidence	-2˚	Main Compartment (MC) Length	20.4 in	Model	Phoenix Edge 100
Static Margin	14.6%	MC Height	4.4 in	Rated Voltage	34 Volts
Vertical Stabilizer		MC Width	4.3 in	Current	100 amps
Airfoil	NACA 0011	Empennage Length	7.1 in	Mass	72.9 g
Height	7.08 in	Empennage Height	6.3 in	Controls	
Root Chord	6.99 in	Empennage Min. Width	17.5 in	Transmitter	T10J 10 Channel
Tip Chord	4.35 in			Receiver	R3008sb
Area	34.32 in^2			Battery	Tenergy 2000 6v

AR	5.86
Leading Edge Sweep	33.12˚

Weight	42.7 g
Servos	HS-425BB

4.2 ANSYS Wing Analysis

The team performed a static structural analysis of the wing assembly using Ansys Mechanical. This was performed using half of the wing assembly to simplify the analysis. This approach provides an accurate analysis since the wing is completely symmetrical and fixed in the middle. The analysis was performed with a total force of 13.5 pounds and was conducted in 2 different ways: with the load concentrated at the wingtip and with the load distributed across the entire span. The analysis was based on 23,609 elements with an average surface area of $1.5*10^{-3}$ m^2. Given a total aircraft weight of about 7 pounds, this analysis includes a safety factor of about 3.86.

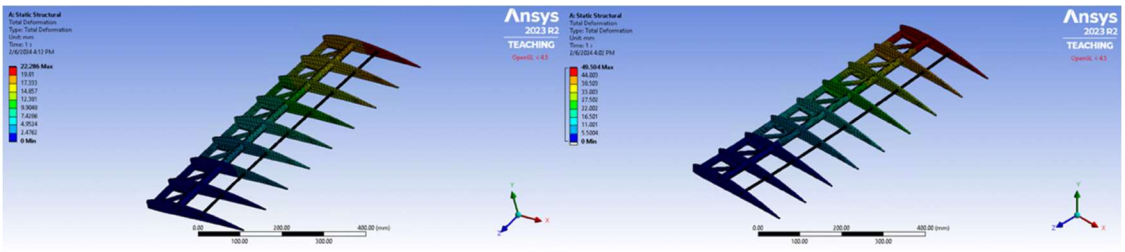

Figure 29: Displacement for ANSYS static structural analysis of wing assembly.

The concentrated force at the wingtip gave a maximum displacement of 1.95 inches. However, the much more realistic analysis using a distributed load showed a maximum displacement of approximately 0.88 inches.

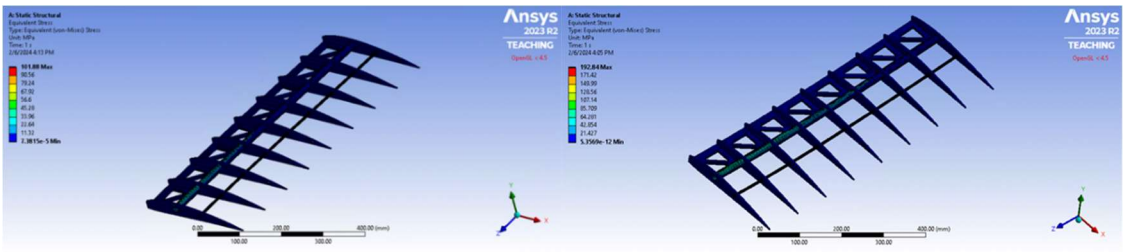

Figure 30: Equivalent stress for ANSYS static analysis of wing assembly.

The maximum equivalent stress in the wing structure is 14.8 KSI for the distributed load, and 28 KSI for the concentrated load. This stress is concentrated almost entirely in the main wing spar, so this magnitude of stress is not a concern.

The ANSYS analysis of wing deflection produced results that are significantly different from the hand-calculated wing deflection analysis in Section 3.5.2. This is due in part to the wing spar dimensions being slightly different. Throughout the design process, the exact dimensions of the wing spar varied slightly based mainly on the availability of products for the team to purchase for the wing spar. The ANSYS analysis was done using a slightly different design iteration wherein the inner diameter is 0.60 inches, and the outer diameter is 0.75 inches. Another reason for the varied results is that the ANSYS analysis calculates deflection at every point in the wing assembly, whereas the deflection in Section 3.5.2 is calculated only for the main wing spar. As shown in Figure 29, the maximum deflection is in the rib at the wingtip, not in the main wing spar. Lastly, the load applied to the wing in both ANSYS simulations was 60 Newtons, or about 13.5 pounds which is significantly more force than the calculations done in Section 3.5.2.

4.3 Controls

This section details all moving components including flaps, ailerons, the elevator, the rudder, and the rear landing gear, as well as their methods of actuation. It is important to note the use of a Futaba T10J 10 channel transmitter and its corresponding receiver, the R3008sb, as well as HiTEC HS-425BB servos. These servos output at 3.3kg-cm. The T10J in combination with the R3008sb allows for the programming of a radio failsafe which automatically initiates when signal from the transmitter is lost to the receiver. During this failsafe, the receiver commands the actuation of full right rudder, full right aileron, full flaps down, full elevator up, and throttle completely closed. The receiver batteries are housed in the front of the fuselage and are connected to a switch that is externally accessible.

4.3.1 Ailerons & Flaps

To give the aircraft the ability to roll, 2 Ailerons are mounted 3.38 inches from the tip of our wing, with a length of 13.38 inches and a chord of 1.5 inches. This provides the aircraft with enough authority to complete the required mission course. The ailerons are actuated by 2 servos

located between 2 ribs of the wing, as pictured in Figure 31. These servos interface with the RC receiver through the use of a Y-splitter. The ailerons are manufactured from .75-inch balsa wood and are connected to the servos via size 2-56 threaded control rods.

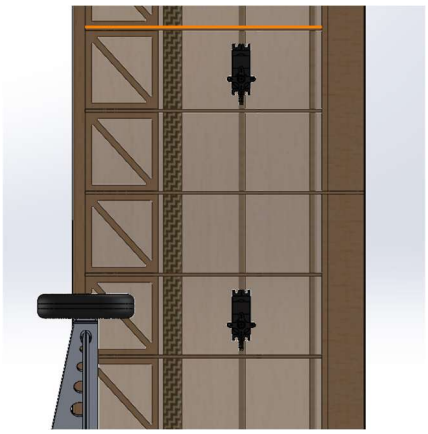

Figure 31: Location of the servos on the wing. (Left is leading edge of the wing).

To achieve a take-off distance of 20 feet, the team elected to include flaps in the wing design. The flaps are placed from the fuselage to the third rib of the wing. In a similar fashion to the ailerons, the flaps are actuated by two servos linked through a y-wire and run into the RC receiver. These servos are housed between two ribs in the wing. The flaps are made from the same material as the ailerons and are connected to the servos in a similar fashion.

4.3.2 Elevator, Rudder, and Rear Landing Gear

To control the pitch of the aircraft the horizontal stabilizer is equipped with a 15-inch elevator. The elevator is actuated by a servo that is housed in the fuselage. A size 4-40 threaded control rod runs from the fuselage to the horizontal tail and is supported by 3-D printed struts. The struts are connected to one of the two tail booms.

The yaw of the aircraft is controlled by the rudder, which is attached to the vertical stabilizer of the aircraft. The rudder is made of 2 0.125-inch pieces of balsa, adhered to each other with perpendicular grains. The rudder is designed in the shape of an upside-down L, as shown in Figure 32.

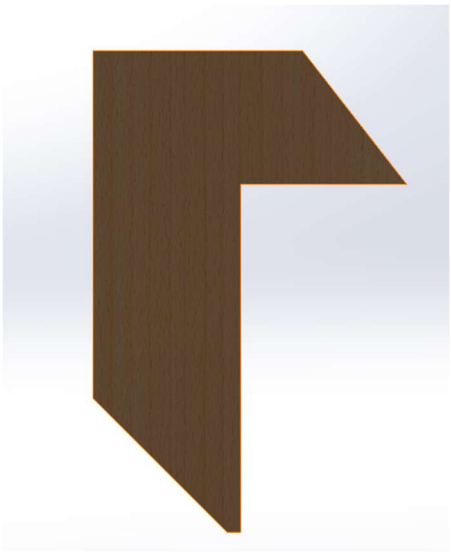

Figure 32: Figure of rudder shape.

This design ensures additional rigidity, as the moment caused by airflow hitting the control surface is coupled on either side of the vertical stabilizer. With a chord length of 3 inches and span of 7.1 inches, the rudder is actuated by a servo housed in the fuselage. Similar to the elevator, a size 4-40 threaded control rod runs from the fuselage to the vertical tail and is supported by a different set of 3-D printed struts connected to the other of the two tail booms. Because a push-pull setup is being used, the control surface actuates more in one direction than the other. To account for this, the RC Transmitter was tuned to limit the amount the rudder can actuate in each direction.

The rear landing gear selected was a Tiger 30cc from Hangar 9. The one-piece axle allowed for easy manipulation of the shape. This allowed the axle to be routed upwards through a hole in the elevator and connect to the trailing edge of the rudder. This design provided the rear wheel with the ability to turn when the rudder is actuated.

4.3.3 Throttle Control

To control the power delivery to the motor, the Phoenix Edge 100 ESC was used. This controller includes a 5-Amp battery eliminator circuit (BEC). To comply with the regulations of the competition, the BEC was disabled, and a 100 Amp arming fuse was added between the battery and ESC. The ESC is routed through the RC receiver and mounted to the lower-front surface of the aircraft's exterior. This allows for the airflow to cool the ESC, as it can overheat during extended use.

4.4 Sub-System Design Integration

4.4.1 Fuselage Integration

The main considerations for the fuselage design were to have a strong connection point for all components of the aircraft and to have sufficient volume to complete all the missions. The fuselage was split into two compartments. The top compartment houses the main structural components such as the mounts for the wing, tail, and landing gear. The bottom compartment houses the aircraft battery. Figure 33 shows the fuselage. The electronic speed controller (ESC) is mounted on the outside of the battery compartment, as pictured below, allowing for the ESC to be air-cooled.

In Figure 33, there are two key details. The landing gear is mounted at the leading edge of the wing. This is essential for a tail dragger configuration as it allows the tail of the aircraft to lift off before the main body of the fuselage. The battery is also mounted as far forward as possible on the aircraft. This helped maintain the center of gravity under the main wing spar.

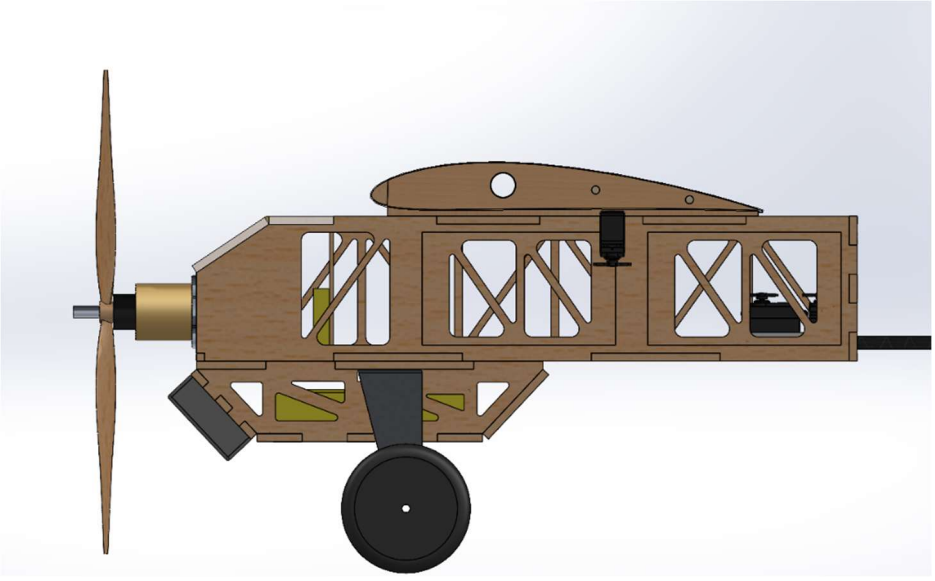

Figure 33: Fuselage.

The fuselage acts as a key structural component requiring a rigid wings mount, tail boom, and landing gear mounting plate. A strong firewall is also required to counter the thrust generated by the motor.

In Figure 34 below, the firewall design is detailed. A thin piece of aluminum, with a thickness of 0.0165 inches, (pictured on the right) was formed into shape. It was fit between two

pieces of quarter-inch thick Lauan wood. On the sides of the motor mount, sheet metal screws were used to fasten the aluminum sheet in place. This design allowed for a distribution of load across the fuselage, reducing the risk of motor damaging the nose of the aircraft.

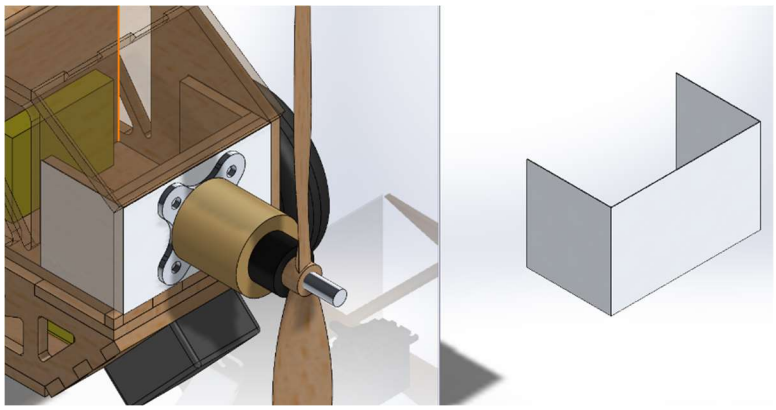

Figure 34: Firewall description.

The mounting of the wing required extra consideration to comply with 2.5-foot-wide parking lot requirement that was imposed by the DBF rules. The wing is mounted with three screws that fasten the wing, secured with T-nuts on the inside of the fuselage. The wing has a 0.25-inch-thick plate of plywood between the bottom of the wing and the top of the fuselage to ensure the wing is at the correct incidence angle. In Figure 35, the 3 blue dots represent the locations of each of the screws.

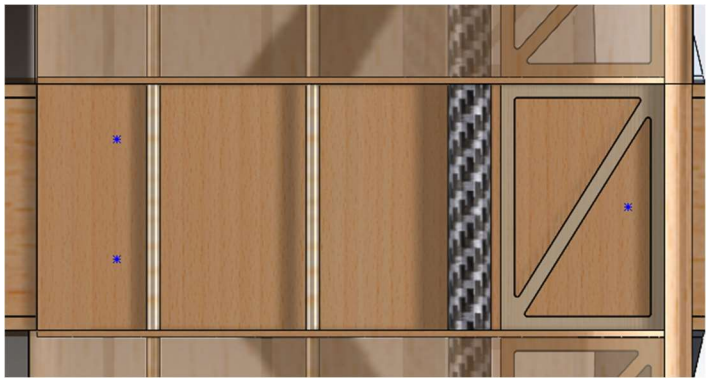

Figure 35: Wing mount description.

The tail boom coupling is another important aspect of the fuselage design. Since the design uses a boom to connect the tail to the rest of the aircraft, two carbon fiber rods were secured to the back of the fuselage, as pictured in Figure 36. The dual-boom design allows the tail to resist torsion during flight. This keeps the plane steady and creates a stronger connection.

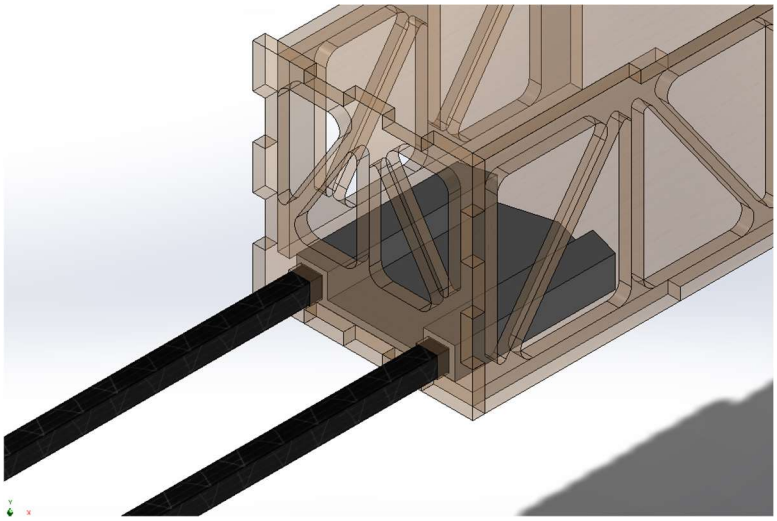

Figure 36: Tail boom connection to fuselage.

The walls of the fuselage are joined as pictured in Figure 37. This increased the surface area for adhesives, making the connections stronger. Epoxy was used to connect the pieces of the fuselage. This also increased the fuselage's resistance to torsional loads generated by the propellor.

Figure 37: Fuselage wall connection.

The location and construction of the landing gear mount serves a critical purpose. Because of the tail dragger design the location of the front wheels will greatly influence the rotational point during take-off. The landing gear is mounted on the same longitudinal position as the leading edge of the wing. The team was also concerned with impact shock experienced during landing. Following recommendations from previous DBF competition teams, the faceplate for the landing gear was reinforced, which allowed it to absorb greater shock loads.

4.4.2 Wing Integration

The wing was designed to have one carbon fiber rod as its main wing spar. This allowed for a lightweight structure with significant strength, as the load would be transferred along the complete wingspan. Additionally, the wing was designed to have two wooden dowels, as shown in Figure 38. For additional strength, the wing was designed to have a leading-edge balsa D-tube.

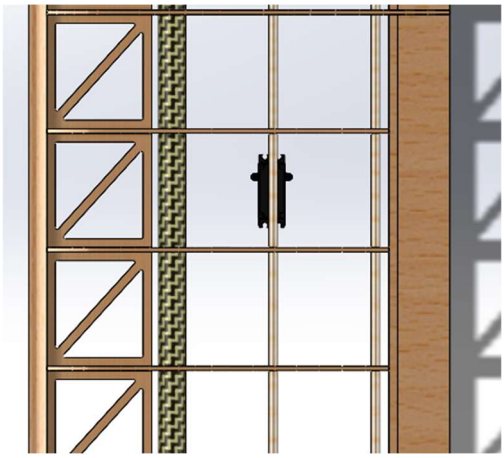

Figure 38: Wing and spar structure with leading-edge D-tube (Left is front*)*.

The wing was designed to have 16 bays that were 3.25 inches wide and 1 bay that was 4.4 inches wide that allowed the wing to rest on top of the fuselage. The wing ribs were made from basswood, with the grain running from leading edge to trailing edge to improve lateral strength.

To further increase the strength of the wing, a balsa D-tube was placed at the leading edge along the entire span of the wing. The D-tube was selected as the best way to improve the stiffness of the wing without adding a significant amount of weight.

An analysis of the wing assembly revealed that it was still not as stiff as desired. This was tested by holding the wing tips and applying torsional loads to see the response from the wing. During the test, the wing did not offer a lot of resistance to the applied loads which lead us to the conclusion that additional support to was required. To further stiffen the wing, a plywood support was added between each rib, except for the center bay where the wing attaches to the fuselage, shown in Figure 39. This piece measured 3 inches by 3.25 inches by 0.25-inch-thick. Lightening holes were added, and the support piece was attached horizontally between each rib using epoxy.

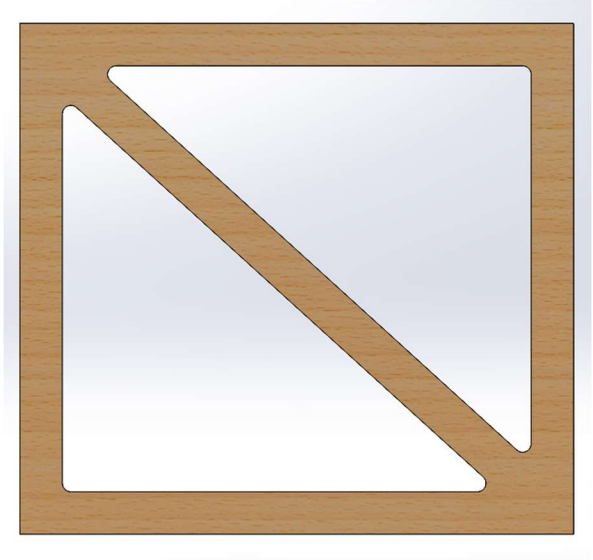

Figure 39: Wing Brace.

4.4.3 Tail Integration

To reduce unnecessary weight, the team decided to have two carbon fiber tail booms connected from the fuselage to the tail. This configuration was chosen because it allowed for torsional rigidity and because of the low weight and high strength of carbon fiber.

To connect the tail booms, a 3D printed component was created, pictured in Figure 40. The tail boom coupling would allow for the vertical and horizontal tail stabilizers to connect without restriction to the motion of the control surfaces. The same 3D-printed part was used to connect the tail booms to the fuselage. The 3D prints were made from standard PLA.

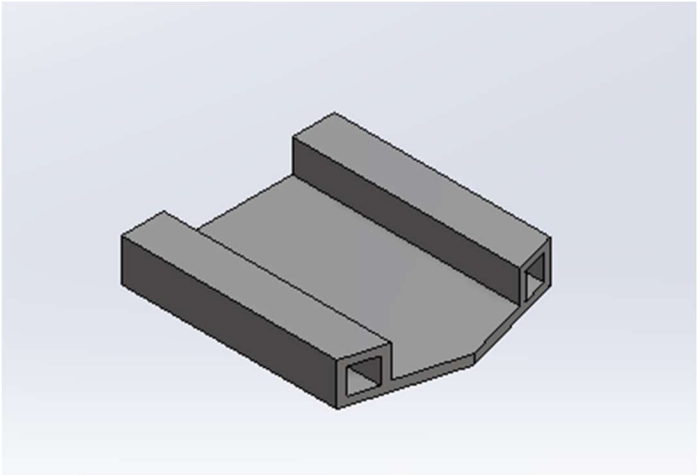

Figure 40: Tail boom coupling.

The vertical and horizontal stabilizers were made from 0.125-inch-thick balsa wood, with two sheets glued together and their grains perpendicular to each other. This allowed for uniform strength without a significant increase in weight.

4.4.4 Landing Gear Integration

The landing gear was secured with four screws threaded through T-nuts to the body of the fuselage. The mounting plate is constructed out of a 0.25-inch-thick piece of plywood mounted internally to the fuselage, increasing rigidity. The landing gear bracket was constructed out of 0.125-inch-thick aluminum with 4 pairs of lightening holes. Horizontal strengthening rods were added to increase the rigidity of the landing gear.

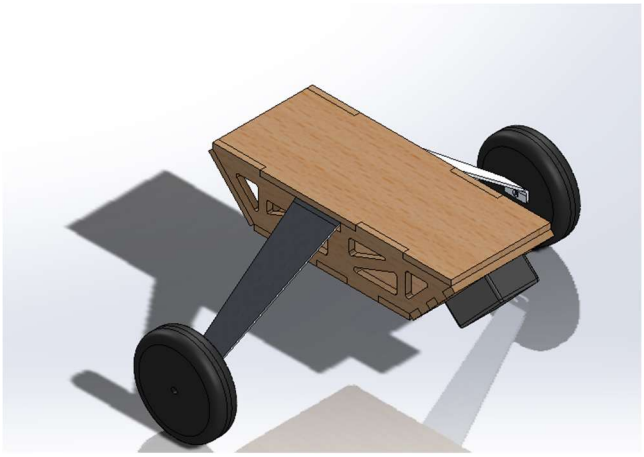

Figure 41: Landing gear mount and battery.

4.4.5 Mission Inserts Integration

To restrain the passengers and payload during flight, three inserts were created for their respective missions. The missions require 2 crew members to fly in the front compartment of the aircraft. A CAD model, shown in Figure 42, was created to fit inside this compartment, which included the receiver batteries and firewall. Additionally, the inserts raised the height of the crew members to ensure they had a line-of-sight over the aircraft motor. A restraint system, which included the top and side wall pieces, was created to ensure that the crew did not move during flight or landing.

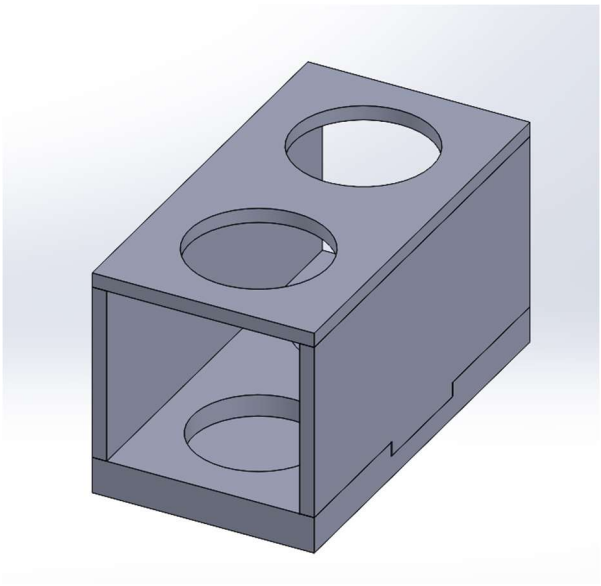

Figure 42: Crew insert.

Mission 2 required 2 EMT personnel, a patient on gurney, and a medical supply cabinet within the rear compartment to fly. A CAD model, shown in Figure 43, was created to fit inside the rear compartment, which included the landing gear base and the tail attachment piece. It had restraint systems, which included the side walls and top piece, to ensure that the payload did not move during flight or landing. A separate CAD model was created for the gurney itself. It had 2 gaps on the bottom to allow for Velcro straps to restrain the patient.

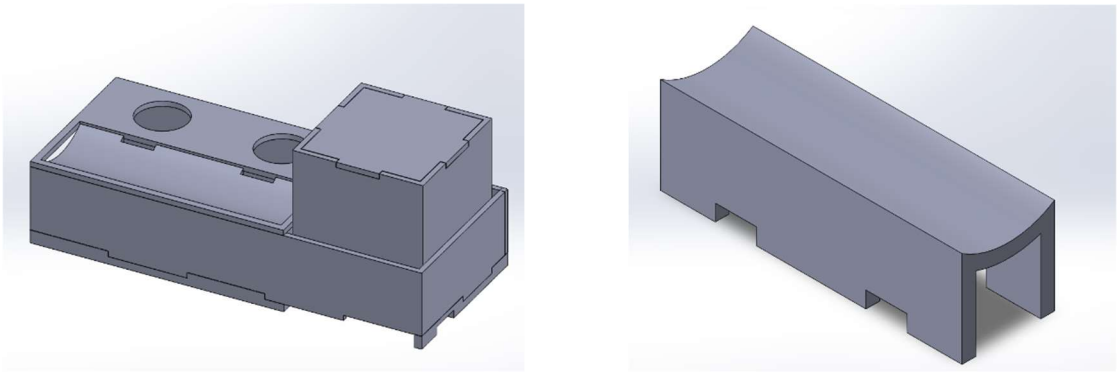

Figure 43: Mission 2 insert (left) and patient gurney (right).

Mission 3 required at least one passenger in the rear compartment to fly. A CAD model, shown in Figure 44, was created to fit inside the rear compartment. For this iteration, the insert can hold up to 10 passengers, with restraints to ensure that the passengers did not move during flight.

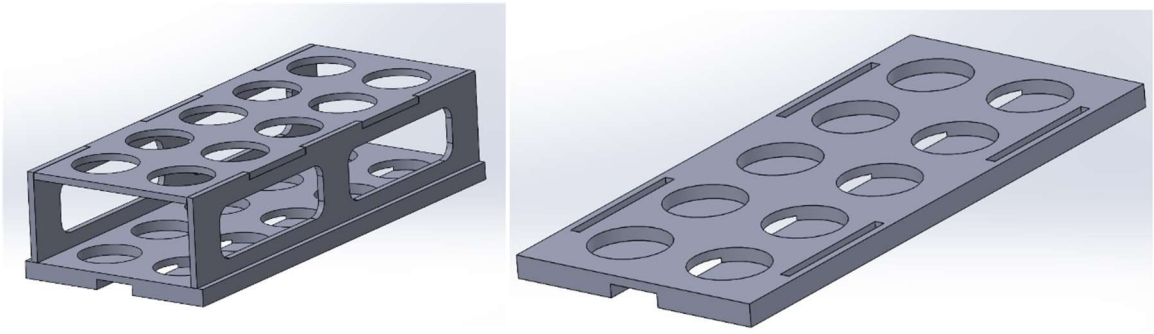

Figure 44: Mission 3 insert and restraints (left) and floor insert (right).

4.5 Flight Performance

As detailed in the mission sequence, the aircraft must have the capability of performing 180° and 360° turns. To ensure the aircraft's capability in performing the turns effectively and safely, a maneuverability analysis was conducted. This included finding the minimum radius and rate of turn at various flight velocities while taking into consideration the load factor of 2 estimated from the maximum load factor of the stall limit.

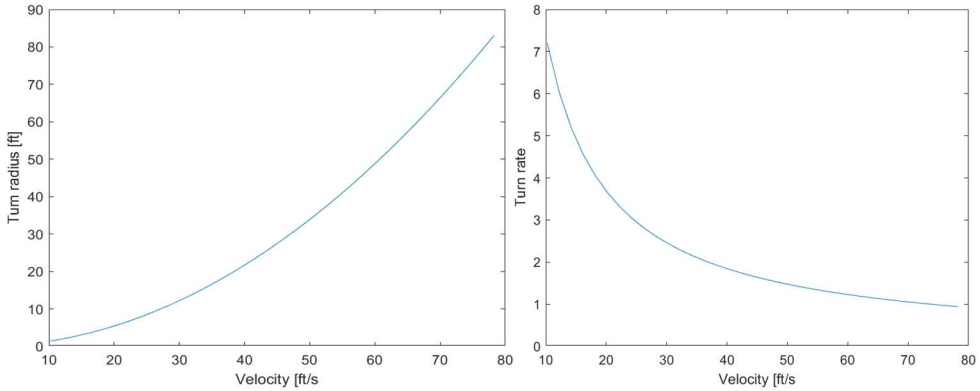

Figure 45: Plot of the turn rate and radius vs velocity.

Figures 45 depict the predicted level turn rate and radius characteristics of the aircraft. To complete the missions as quickly as possible, it is crucial that the aircraft can withstand sharp turns. This will help optimize mission performance while conducting the required mission maneuvers.

5 Manufacturing Plan

The following section describes the manufacturing processes and materials used for the construction of the aircraft.

5.1 Manufacturing Process

The team utilized several processes to manufacture and assemble the aircraft, including laser cutting and 3D printing.

5.1.1 Laser Cutting

To ensure precise manufacturing and create a cohesive structure, the team modeled the wooden components in SolidWorks and then combined them into an assembly. Drawing files were created for each part and downloaded as an image file. For the duration of this project, there were two available laser cutting machines at WPI: the Full Spectrum Pro Laser 48”x36” 120W and the Full Spectrum Pro Laser 24”x16” 90W. Both laser cutters used the Retina Engrave software, which allowed the team to import the image files and use the tracing tool.
Four different types of wood were used for this project: balsa, balsa plywood, lauan plywood, and basswood. Varying power, speed, and pass settings were used depending on the type of wood being cut. These settings were adjusted experimentally based on the quality of test cuts. Table 12 shows the settings that the team used to cut each different type of wood on the Full Spectrum Pro Laser 24”x16” 90W laser cutter.

Figure 46: Test cuts of balsa plywood using different settings.

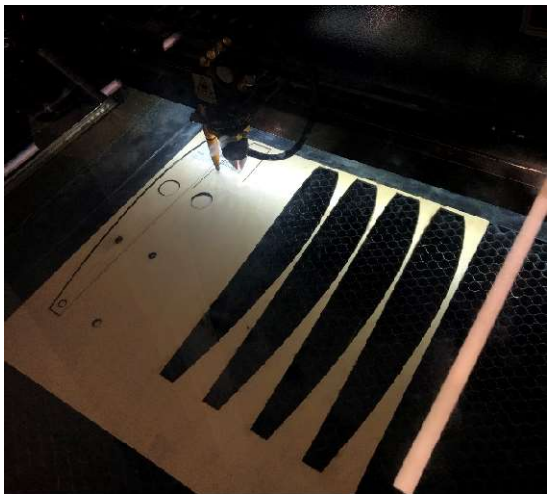

Figure 47: Laser cutting wing ribs.

Table 12: Laser cutter settings

Type of Wood	Power Percentage	Speed Percentage	Number of Passes
Balsa Wood	7%	50%	2
Balsa Plywood	25%	25%	1
Lauan Plywood	25%	25%	2
Basswood	9%	25%	2

5.1.2 3D Printing

Multiple components of the plane were manufactured using a 3D printer: the tail boom struts, the tail boom coupling, and the mission inserts. The parts were created in SolidWorks and added to the assembly. Parts were also adjusted for tolerances, as 3D printing filament is susceptible to fluctuations in size. For this project, 3D printers at WPI as well as a personal 3D printer were used: the Ultimaker 3 Extended, the LulzBot TAZ Workhorse, and Ender 3. 11 parts were printed using PLA filament, although TPU was used for a prototype for the mission inserts.

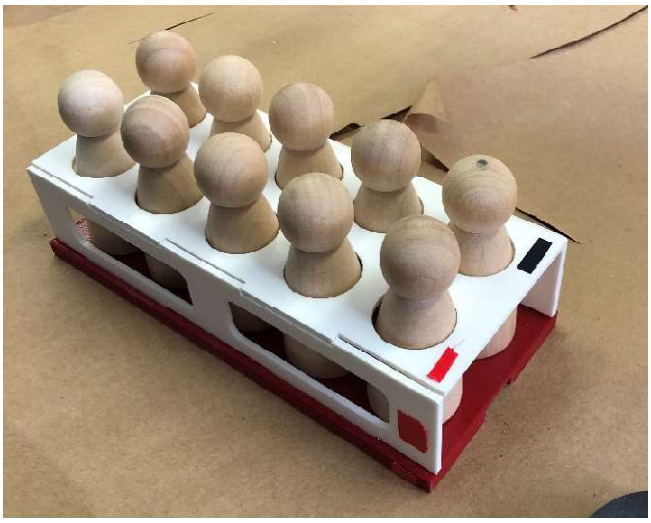

Figure 48: Assembled mission 3 insert with passengers.

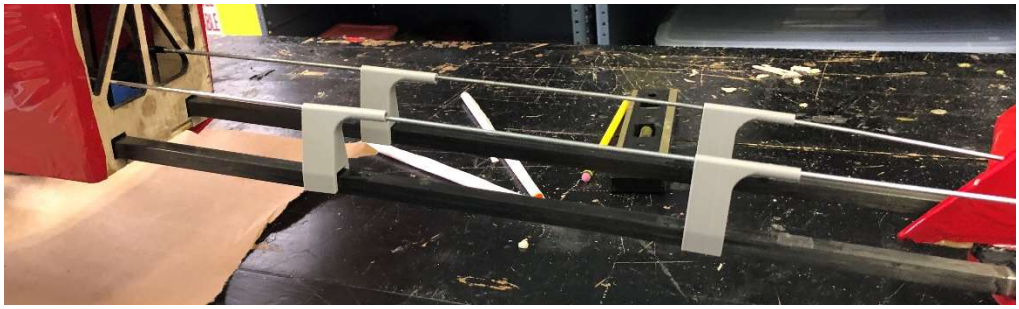

Figure 49: Tail boom struts attached to aircraft.

5.1.3 Adhesives

Several types of adhesives were used to attach the aircraft components together. For wood-to-wood connections, wood glue was mainly used. However, some laser cut components required 30 minute- Z-Poxy epoxy due to the carbon residue on the gluing surface. Components were glued and clamped together for a 24-hour period before any stress was applied. For any other type of connection (wood to carbon fiber, wood to plastic, or wood to PLA filament), either epoxy or Loctite Professional Liquid cyanoacrylate glue was used depending on the exposure to flight conditions. For example, cyanoacrylate glue was used for any components that were internal, such as bulkheads. 30-minute Z-Poxy epoxy was used for any parts that were external. Velcro was used to attach hatches to the aircraft. The Velcro had an adhesive back which was directly applied onto the surface. JB Weld was used for attaching the landing gear support.

Figure 50: Adhesives used to attach aircraft components.

5.1.4 MonoKote

MonoKote is a plastic shrink wrap film that was used to cover the entire plane to reduce drag, and to cover the gaps between the fuselage parts, the wing parts, and the tail parts. To apply the MonoKote, the team used a heat iron on a low setting to attach it onto the surface. Then a high heat setting was used to shrink the MonoKote until it was to the proper shape and size.

Figure 51: Aircraft with red MonoKote.

5.2 Manufacturing Overview

The construction of the aircraft was divided into several areas, including the construction of the wing, fuselage, tail, and mission inserts.

5.2.1 Wing Construction

Basswood was used for the ribs of the wing due to its strength and low density. Balsa wood was used for the D-tube, horizontal bay supports, control surfaces, and coverage of the wing. The control surface and the leading-edge piece were commercial off-the-shelf pieces purchased from a local hobby shop. The balsa wood that covered the wing was 0.03125 inches thick. The balsa wood for the horizontal bay supports were laser cut.

Figure 52: Horizontal braces added onto wing ribs using wood glue.

To add more connection points and to create a rigid structure that did not twist under load, a carbon fiber and aluminum wing spar as well as two wooden dowel pins were used. The carbon fiber rod was 0.77 inches in outer diameter, and aluminum was added on the ends to create the necessary wingspan length of 58 inches. The wooden dowels were 0.25 inches in diameter. All three spanned the entire length of the wing; none were interrupted by the control surface.

Figure 53: Assembled wing prior to MonoKote.

5.2.2 Fuselage Construction

Lauan plywood was used for most components of the fuselage. The fuselage utilized a box joint construction to maximize the gluing surface and to ensure the joints are orthogonal. Additionally, the design of the joints helped prevent wood warping, which occurred frequently. The fuselage was attached using wood glue, with minor sanding needed for the pieces to fit together. Lightening holes were added as pictured in Figure 54. There were no lightening holes on walls that were facing the direction of flow to maximize strength.

Figure 54: Partially assembled fuselage with lightening holes.

5.2.3 Tail and Tail Boom Construction

To connect the fuselage to the tail, two pieces were created. The tail-side boom coupling had a slot for the vertical stabilizer. The fuselage-side boom coupling allocated space for the

servo mounts. Both pieces were created on SolidWorks and then 3D printed using PLA filament. The horizontal and vertical stabilizers and their corresponding control surfaces were made from balsa wood. There were no lightening holes added to ensure maximum strength. Carbon fiber square rods were used to connect the tail to the fuselage. Since the distance between the tail and the fuselage was 17.5 inches, the tail control rods buckled in flight. Thus, tail boom struts were created and attached onto the carbon fiber rods.

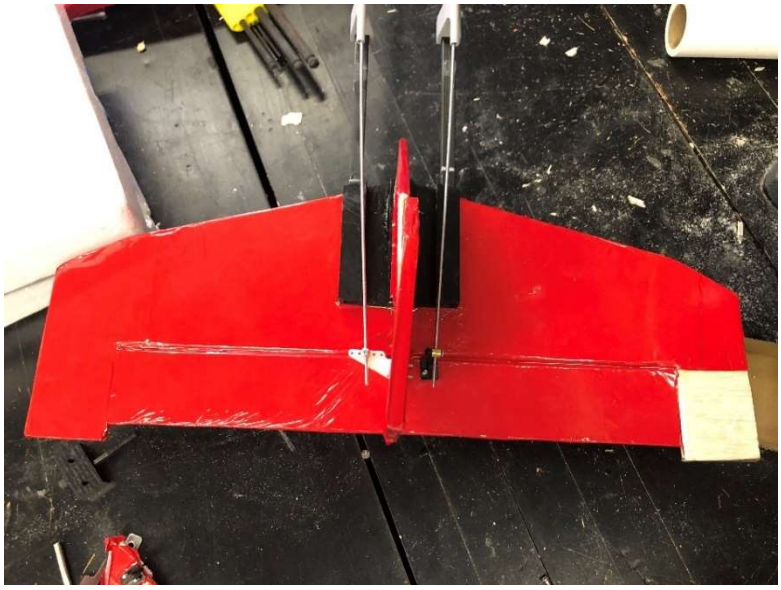

Figure 55: Assembled tail with MonoKote.

5.2.4 Mission Inserts Construction

Fuselage inserts were created specifically for each mission, and a crew insert was created for use in all 3 missions. The team chose to place the medical supply cabinet forward of the patient on gurney and EMTs for Mission 2 as it limited the change in center of gravity. The medical supply cabinet had the minimum dimensions of 3 inches cubed. The gurney was modeled to be the exact dimensions of the patient. For Mission 3, the internal dimensions of the fuselage allowed the team to fit 10 passengers arranged in 5 rows of 2. All mission inserts were designed in SolidWorks and 3D printed using PLA filament. Mission inserts were attached to the fuselage using Velcro.

6 Testing Plan

Beyond simulation and theoretical analysis, the aircraft was also physically tested to ensure it performed as expected. For flight testing, the team partnered with the Central Massachusetts Radio Controlled Modelers (CMRCM) Club to perform testing at their field in Northborough, Massachusetts. This location provided a grass runway and a FRIA compliant location for legal and safe flight testing.

6.1 Sub-System Testing

6.1.1 Aerodynamic Testing

The scaled wing tests were performed in a low speed, low turbulence wind tunnel with a one-foot square test section. Analysis was conducted on wings with varying camber and thickness to optimize our take-off distance by maximizing our lift production. The wings were tested at a cruise speed of 98ft/s where data was collected at angles of attack ranging from -5 to 17 degrees with 3-degree increments. At each angle of attack increment, the pitching moment, normal force, and axial force were recorded. This data was used to find the aerodynamic coefficients of the forces and moments acting on the wing. Figure 56 displays the wind tunnel test configuration.

Figure 56: Aerodynamic wind tunnel.

6.1.2 Propulsion Testing

Propulsion system testing was completed with the use of an RCBenchmark motor test stand which provided data for thrust, torque, and power output. Preliminary research was already used to determine what motor would be used, thus thrust testing focused on propeller selection. With the motor secured to the test stand several propellers were attached and subsequently run for both 15 seconds and 1 minute at full power. After each test, peak wattage, average wattage, flight controller amperage and peak thrust were recorded. Final propeller design was determined by the layout that produced maximum thrust while keeping amperage at 70% of the flight controllers maximum rated amperage to ensure propeller cooling and flight time.

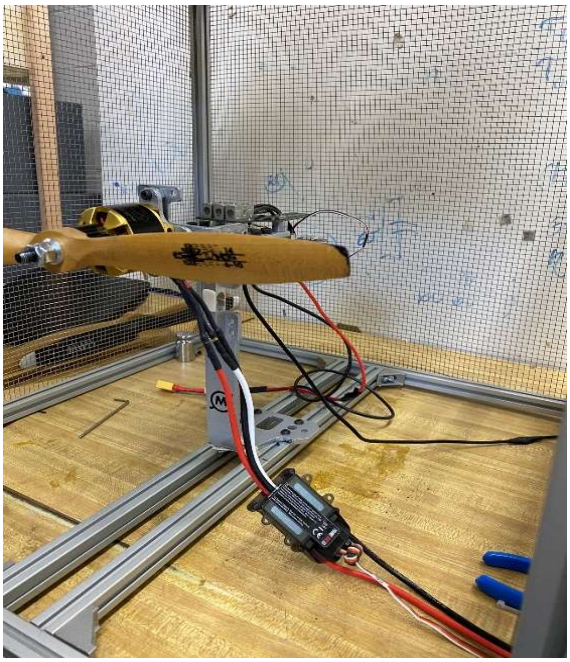

Figure 57: Propulsion system testing.

6.1.3 Structural Testing

The following tests were conducted before each flight test to ensure the safety of the team members and the pilot. A failure of any one of these tests would prevent the aircraft from flying until adjustments were made.

6.1.3.1 Firewall Test

To test the firewall before flight, the aircraft was restrained with two supports on the wing. When the plane was secure and in the flight configuration, the team moved to a designated

area behind the plane to ensure safety. The motor was then turned on. The power to the motor increased gradually, until it reached full power. This ensured that the firewall and motor mount could withstand the load from the motor. The firewall remained intact throughout the power test thereby reinforcing its structural integrity for flight.

6.1.3.2 Wing Loading

To test the structural rigidity of the wing, a payload of 10 pounds was placed in the fuselage. The aircraft was lifted by the wing tips while under load to check for a large deflection or potential failure of the wing.

6.1.3.3 CG Test

The center of gravity was tested in two planes. First, two team members picked up the plane by the wing tip. The team members then worked together to balance the plane from the wing and confirm that the center of gravity was located near the quarter chord point of the wing. The plane was then lifted by the motor and the tail to check for a rolling moment induced by the center of gravity.

6.1.4 Control Testing

6.1.4.1 Servo Configuration Testing

4 servos make up the electronic control scheme. Servos were initially validated by connecting one at a time to a fully charged battery and the same port on the receiver with a force gauge attached. Each servo is then fully actuated, and the peak force generated is recorded, ensuring all servos are working within specifications. All 4 then connect to separate ports on the receiver simultaneously and are configured within receiver software to align to their respective control surface. Software tuning is used to determine actuation limits of servos respective to accompanying control surface. All controller inputs are tested before flight ensuring correct control scheme.

6.1.4.2 Failsafe Test

Electronic failsafe procedure is tested through two faults. The first fault is tested by disconnecting the receiver battery on the aircraft simulating a loss of power to the control

surfaces. In this situation, motor power is also removed as signal wire from the flight controller has been removed disabling the ability for the flight controller to control motor power without input from the RC receiver. The second fault is tested by turning off the RC controller simulation a loss in controller and receiver connection. This fault is programmed into the receiver logic and directly follows AIAA DBF rules. With use full right rudder, full right aileron, full flaps down, full elevator up, and throttle completely closed.

6.1.4.3 Range Test

A range test for the transmitted was performed as both a requirement for the technical inspection of the competition and to ensure the functionality of the aircraft. The test is performed by launching the transmitter into low-power mode. This is done by holding down the menu button and switching the controller on. The low power mode does not allow for the throttling of the motor but does allow the servos to be tested. After booting into low-power mode one team member with the transmitter walks ~50 feet away and tests each servo using the transmitter.

6.2 Flight Testing

6.2.1 Flight Testing Checklist

Table 13: Flight Checklist

Preflight		Before Takeoff	
Assembly		Takeoff Warning	DECLARED
Wing	SECURE	Throttle	100%
Empennage	SECURE	Control Surfaces	UNINHIBITED
Motor	SECURE	Flaps	AS NECESSARY
Propeller	SECURE	Runway	CLEAR
Batteries	SECURE	Propeller Path	CLEAR
Landing Gear	SECURE	Pre-Landing	
Center of Gravity	¼ CHORD	Runway	CLEAR
Airframe		Flaps	DOWN
Crew	SECURE	Landing Warning	DECLARED
Mission Insert	SECURE	Post-Landing	
Mission Payload	SECURE	Throttle	OFF
		Radio Controller	OFF

Batteries	DISCONNECTED
Aircraft	INSPECT

6.3 Flight Testing Results

All flight tests were conducted at the CMRCM field. The field provided a safe and legal place for the aircraft to be tested.

6.3.1 First Flight Test

The first flight test revealed a particular sensitivity to rolling moments, causing instability. This aerodynamic flaw prevented the airframe from sustaining banked turns or steady level flight. Stability issues became more drastic as airspeed increased, thus only 20% of the motor's power was tested to keep the aircraft maneuverable. Post-flight analysis revealed significant buckling in the control rods connecting the rudder and elevator servos to their respective control surfaces. Adding 3D printed struts, as pictured in Figure 58, along the tail boom increased the rigidity of the control rods to allow for accurate control. Upon review of the footage, the aircraft displayed a tendency for the airframe to nose up under power. As a result, the incidence of the motor was decreased.

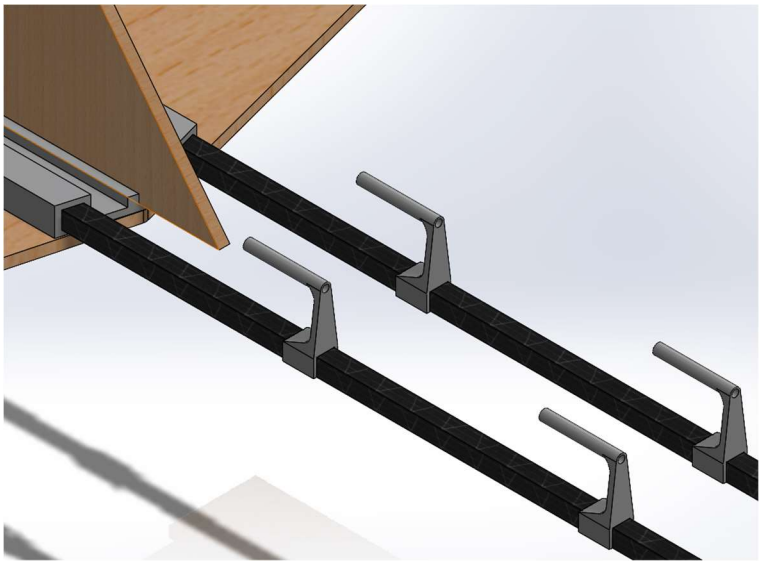

Figure 58: 3D printed struts to increase rigidity of control rods.

Figure 59: Aircraft in flight.

6.3.2 Second Flight Test

The second flight test's purpose was to examine if the modifications applied to the aircraft had corrected the rolling instability from the first flight. The test revealed even greater problems. The pilot reported that the airframe was "unflyable" and had "serious issues in the aileron". Post-flight analysis and discussion with the pilot revealed two key issues. The first issue was that the motor's incidence was over-corrected, which increased instability. Secondly, because of the motor's incidence, airflow was rapidly accelerated and pushed across the bottom of the aircraft wing. This created a drastic pressure differential, generating an updraft at the trailing edge of the wing. When the ailerons were fully actuated, this updraft generated enough force to push the servos past 90 degrees and locked them in position. This made the aircraft unresponsive. Changing the rotational point of the servo ensured that even in the event of an over-actuation, the servo arm would not move past 90 degrees, allowing the servo and subsequent control surface to return to center.

6.3.3 Third Flight Test

The third flight test demonstrated excellent results. Modifications from the first two rounds of testing provided the airframe with the stability and performance required to complete all 3 missions. The airframe also demonstrated considerable agility, allowing the aircraft to perform rolls, loops, and even fly inverted. The pilot also described the aircraft as "easy to fly"

and “able to take-off and land repeatedly without an issue”. With this configuration, the airframe is expected to perform well within the required performance characteristics for the DBF competition.

6.3.4 Fourth Flight Tests

The fourth flight test was conducted to test the aircraft’s mission performance with the inclusion of flaps. The integrity of the inserts for the 3 missions was another aspect of assessment. During the flight test, a full throttle take-off was attempted. The rudder was not able to counteract the torque generated by the motor leading the aircraft to make a 90 degree turn to the left. The pilot managed to get the plane off the ground; however, at full power the plane flew straight upwards. The pilot backed off the throttle to level out the plane. An over correction was made causing the plane to nosedive into the ground. This resulted in severe damage to the propeller, rendering it no longer usable, and the fuselage compartment. Post-flight analysis and discussions revealed that the performance of the plane was still excellent, however, a take-off strategy needed to be addressed. A full power take-off was deemed impossible for the size of our aircraft and rudder size. Based on this experience, it was decided that adopting a roll-on take-off approach where the power is gradually increased with flaps engaged was the most viable option for ensuring that the aircraft is able to safely lift off the ground.

Figure 60: State of the plane after flight test.

6.3.5 Fifth Flight Test

The fifth flight test was very successful. It was conducted to test the aircraft's performance with the newly built fuselage as well as recording a proof of flight video for the AIAA competition. Despite the strong crosswinds on the day of the test, the aircraft was able to achieve steady level flight. The pilot did note that the aircraft was resistant to turns due to the formation of vortices along the sides of the leading edge of the fuselage. To mitigate this especially during the competition, performing wider and slower turns was recommended. As noted in the previous flight test, the propulsion system was oversized, making the rudder and aileron sensitive to pilot's input. To prevent the plane from torque rolling during cruise conditions, the pilot recommended operating the motor at half or quarter throttle. During the competition, the team did not have the same pilot flying the plane, therefore, these recommendations were very useful to help the competition pilot become accustomed to the flight behavior characteristics of the aircraft.

7 Conclusion

7.1 Summary

At the beginning of the project, the team split into five teams whose roles were focused on performing initial sizing and design analysis on the various components in the aircraft. This analysis was performed in accordance with the 2024 AIAA DBF rules and mission requirements, guiding the team's approach to creating a conceptual design of the aircraft. Once a conceptual design was developed, extensive analysis was performed to test the aerodynamic efficiency, structural integrity, and stability of the aircraft. The analysis was performed on various software programs to describe the theoretical behavior of the aircraft. Experimental tests on scaled models were then conducted to validate the correctness of the theoretical estimates. Following the preliminary analysis, the manufacturing process of the aircraft was started based on the final configuration of the aircraft from the preliminary analysis. The team used machines such as the laser cutter and 3D printer to manufacture various aircraft components. There were many challenges encountered during manufacturing, but through successive iterations, the team enhanced its capabilities to produce prototypes effectively. The manufactured prototype aircraft

underwent extensive flight testing during which another round of design iterations was carried out to optimize its performance in preparation for the competition.

The team placed 61st out of 107 participants, successfully completing the ground mission and the first flight mission. The second mission was attempted and had a successful takeoff and landing; however, the attempt was disqualified as the judge felt the proper flight course was not followed. An attempt for the third mission was not made, as the team was only called for flight twice during the four-day event. This is largely due to the team's long turnaround on the technical inspection and late placement in the flight order.

7.2 Conclusions from Competition

The aircraft entered for the 2024 DBF flyoff was an aircraft well engineered for flight characteristics without enough emphasis placed on mission eligibility. The flight performance of the aircraft represented a clear success with flight dynamics that allowed takeoff to occur in ~15 feet even when loaded with our aircraft heaviest payload. One area of improvement that could be noted during the competition was the power balance of the aircraft. The propulsion system was clearly oversized for the weight class of the aircraft and required on-site adjustment to ensure stable and safe takeoffs during the competition.

Mission performance is another key takeaway. During the competition, several key mission parameters and components had to be redesigned or modified to properly adhere to different mission specifications. This not only delayed the team's ability to pass technical inspection, but also severely hindered the team's scores in the ground mission as the loading and unloading of different mission sets was slow and inefficient. This also added increased strain to the ground crew as the aircraft needed to be staged for flight within a 5-minute window. The inefficiency of the loading mechanism led to the staging times being in the 4-minute and 30 seconds range, leaving very little time to ensure that everything on the aircraft had been established correctly. A more serious focus on engineering mission eligibility would have gone a long way to ensuring a better performance for the aircraft.

Lastly, the importance of having a pilot familiar with the aircraft became apparent during the competition. While the team was fortunate enough to find a pilot who was willing and able to adapt to the aircraft over the course of a day and a half, it was clear that a properly familiarized pilot is an indispensable asset. Not only will a pilot who has flown the aircraft throughout the

entire design and manufacturing process be familiar with any quirks that the aircraft might have, but they would also be able to inform design decisions based on flight feedback, something the team discovered during the competition as the team modified the aircraft to fit the new pilot's flight style. A pilot capable of traveling to the competition and being present for the entire design process would certainly increase the performance of the aircraft at the competition as you would not have to worry about pilot familiarization on site.

7.3 Recommendations for Future Work

Drawing from the successes and challenges throughout the project, this section offers recommendations to assist future teams. At the beginning of the project, it is important that team members familiarize themselves with analysis software such as XFLR5, ANSYS and MATLAB or Excel, design tools such as SolidWorks, and acquire certification to use manufacturing machines such as the laser cutter and 3D printers. During the aircraft design process, Raymers text, Aircraft Design: A Conceptual Approach along with Lennon's text "The Basics of RC Model Aircraft Design," offered a lot of guidance on the process of sizing the whole aircraft.

In terms of manufacturing, emphasis should be placed on beginning the process earlier. It is going to take a couple of design iterations to get the right wood and vendors that sell high quality material. Additionally, earlier manufacturing will allow for testing in C term. It will be difficult to test the plane in D term because of adverse weather conditions. When manufacturing the plane, emphasis should be placed on the structural integrity of the fuselage as it absorbs all the impact from landing. Furthermore, manufacturing the whole plane with similar wood is strongly recommended. This will allow for easy manipulation of the center of gravity to the desired position.

For the sake of scoring well in the competition, there are a few key takeaways that the team has learned from competing. First, a strong report is key to scoring well, as its score is used for determining the flight order. The team was 86th for this year's flight order. This meant that the team did not get a chance for technical inspection until the second day of the competition. Second, passing technical inspection on the first try is incredibly important. If a team does not pass technical inspection on their first try, they must wait out the rest of the flight order and wait for all teams that were before them as well. Because of this, the team was not able to pass technical inspection until the third day of competition, leaving time for only 2 flight attempts.

Had the team passed technical inspection on the first day of the competition, by both writing a stronger report and paying more attention to the technical inspection checklist, there would have been time for 3 or more flights. Thirdly, focusing on the mission critical aspects rather than on making the best RC plane would help tremendously. The science of making an RC plane is known and does not need to be reinvented. There are some small details worth strong engineering, but generally choosing a basic design that has proven itself and adapting it for the mission would lead to higher scores.

An update to the structure of the teams would also be beneficial to the success of the project. Firstly, having a dedicated pilot who over the course of the project learns how to pilot RC aircraft, first starting on training models, then graduating to sport models, then to the team's RC plane would be greatly beneficial. A pilot involved in every stage of the aircraft's design would be able to understand the unique characteristics of the aircraft and would be able to contribute valuable insights for design enhancements through flight feedback.

In addition to the addition of a dedicated pilot, the team has determined a new structure for future teams: 3 sub-system design teams and 3 manufacturing teams. The 3 sub-system design teams are controls, structures, and aerodynamics. The 3 manufacturing teams would split such that there is one team on the wing, one on the fuselage, and one working on the tail section. Each manufacturing team should receive one member of each sub-system design team. To use the wing as an example, the structure sub-team member would be able to complete an analysis on the structural capacity of the wing, the aerodynamic sub-team member can work to analyze and maximize the wing's performance, and the controls sub-team member can work to determine control surface sizing and logistics. These three team members would also handle the fabrication of the wing to their specifications. The team believes that this would contribute much to the overall design of the plane for two main reasons. First, assigning each team member to a specific aspect of the plane (i.e. one person determines the size of the ailerons) allows for more in-depth research to be completed on that specific aspect of the plane. Structuring the teams in this manner would also allow for the construction of the plane to be completed more efficiently, as there is less waiting for the completion of the other manufacturing team's work. Manufacturing teams can also be held more individually accountable, making up for discrepancies in work among teammates.

7.4 Project Broader Impacts

The theme of the AIAA 2024 DBF competition was to design an aircraft to demonstrate Urban Air Mobility (UAM). This aligned with the emerging aviation market that is seeking to revolutionize transportation utilizing small aircrafts. These aircrafts would be used in the transportation of cargo and passengers around densely populated areas. The design of such an aircraft has tremendous implications in the advancement of urban transportation. For instance, the health care industry will be revolutionized with the implementation of such technology. The ability to access densely populated as well as remote areas due to their small take-off and landing capabilities will provide faster responses to areas faced with disasters, faster transportation time for patients, optimized medical services and organ transportation. The timely delivery of medical services that UAM promises has the potential to save numerous lives.

Apart from health care, this new form of day-to-day transportation can bring a lot of benefits to the economic sector. By utilizing airspace, traffic congestion in cities will be significantly reduced. Additionally, it will improve air quality by reducing emissions from cars with internal combustion engines, thus reducing our carbon footprint. Utilizing UAM aircrafts also has the potential of fostering a more interconnected society by enabling transportation to regions with diverse terrains and reducing commute time to those areas. UAM aircrafts hold great promises for future developments in urban transportation by creating a society with an economy that will be efficient and sustainable.

References

[1] “2023-24 Design, Build, Fly Rules,” American Institute of Aeronautics and Astronautics, 2023.

[2] Raymer, D.P., “Aircraft Design: A Conceptual Approach,” Sixth Edition, AIAA, 2018.

[3] Lennon, A., “The Basics of RC Model Aircraft Design,” Air Age Media, 1996.

[4] “14 Code of Federal Regulations 89.110-230,” United States National Archives, 2024.

[5] “Liperior 5000mAh 5S 60C 18.5V Lipo battery with XT90 plug for RC plane, Retrieved February 23, 2024. https://rcbattery.com/liperior-5000mah-5s-60c-18-5v-lipo-battery-with-xt90-plug.html”

[6] “An Internet Book on Fluid Dynamics,” California Institute of Technology.

[7] 1“The Federal Register,” *Federal Register :: Request Access* Available: https://www.ecfr.gov/current/title-14/chapter-I/subchapter-F/part-89.

APPENDICES

APPENDIX A: MATLAB CODE:Weight Estimation MATLAB Code

```
clc; clear all; close all;
Wp = 6*0.4534 %0.088*5*0.4534; % Weight of the passengers in [lb]
Wc = 0.1556*2*0.4534; % Total weight of crew in [lb]
%h = 0.12192 % Climb altitude in [Km]
Tclimb = 10/(3600); % Climb time 1/2 min [hr]
Pmotor = 1.25; % Used SII 4020 [kW]
Esb = 85; % Specific enegy of litium Polymer battery [Wh/kg]. Used lower
% limit but ranges bten 100-265
nb = 0.93; % Battery efficiency from Historical data
np = 0.90 % Propeller efficiency from Historical data
g = 9.8;
g2 = 35.31485 % Km/hr^2
R =0.9144 % Range in [Km]
LD_ratio = 10; %CL/CD of NACA 4412 at 3degrees AOA
A = 0.2; % Curve fit constant
c = -0.06; %Curve fit constant for Home built aircraft
Wo_guess = 3; % Initial weight guess [kg]
while true
   BMF1 = 0; % Taxi and Take off leg
   BMF2 = ((Tclimb*Pmotor*1000)/(3.6*Esb*nb))*((Wo_guess)) %climb
   BMF3 = (R*g2)/(Esb*nb*np*LD_ratio) % Cruise leg
   BMF4 = 0.005;
   BMF = BMF1+BMF2+BMF3+BMF4
   Empty_Weight_Ratio = A*(Wo_guess^c)
   Wo_new = (Wc+Wp)/(1-BMF-Empty_Weight_Ratio)
   Error = (Wo_new-Wo_guess)/Wo_guess
   if Wo_new < 0
      error('Wo_guess is zero; division by zero error.');
   end
   if Error >= 0.01 && Error <= 0.03
      Wo = Wo_new/0.4534
      break;
   else
      Wo_guess = Wo_new;
```

```
    end
end
```

APPENDIX B: Beam bending analysis MATLAB code.

```
L = 29; %in
outer_diameter = 0.77; %in
inner_diameter = 0.70; %in
t = (outer_diameter - inner_diameter) / 2;
I = 1/2 * ((outer_diameter/2)^2 + (inner_diameter/2)^2);


E = 1305.34; %ksi


w_total = 8; %lbf
w = w_total /L;

n = 100;
x = linspace(0, L, n);


V = -w * (L - x);
M = (w / 2) * (L^2 - x.^2);


V_max = w_total;


A_prime = pi * (outer_diameter^2 - inner_diameter^2) / 8; % Half the cross-sectional area
y_prime = outer_diameter / 2;
Q = A_prime * y_prime;


shear_stress = V_max * Q / (I * t) / 1000;


E_psi = E * 1000; %converting to psi
```

```
delta_max = w * L^4 / (8 * E_psi * I); % in inches



subplot(2,1,1);
plot(x, V);
title('Shear Force Distribution');
xlabel('Length (in)');
ylabel('Shear Force (lbf)');

subplot(2,1,2);
plot(x, M);
title('Bending Moment Distribution');
xlabel('Length (in)');
ylabel('Bending Moment (lbf.in)');

% Display results
disp(['Maximum shear stress: ', num2str(shear_stress), ' ksi']);
disp(['Maximum deflection: ', num2str(delta_max), ' inches']);
```

APPENDIX C: Propulsion test stand data analysis tool in MATLAB code.

```
clear all; close all; clc;

% 15-6  5  Cell  Prop  Test

% initialize thrust data from csv
thrust_data = readmatrix('thrust_data.csv');
thrust = thrust_data(294:609,10);
time = thrust  data(294:609,1);

% from Aircraft
mass = 8.7984/32.2;

% calc accel, then find where the accel is at a maximum
accel = thrust./mass;
[maxaccel, indexA] = max(accel);

% Time starts when max thrust, lasts five seconds
t0 = time(indexA);
tf = time(indexA) + 5;
trange = tf-t0;
tspan = linspace(0,trange,numel(accel));

% integrate to find velocity during that time
for i = 1:numel(accel)
```

```
    vel(i) = accel(i)*tspan(i);
end

plot(tspan,vel)
```

APPENDIX D: Aircraft Drawing Package

The drawing package contains a configuration drawing with a dimensioned 3-way view, a structural arrangement drawing with a Bill of Materials, a systems layout drawing, and a payload accommodation drawing. Three parts were used from GrabCAD, which were the propeller, the servos, and the control horns. The propeller was created by Dhairya Patel, the servos were created by Can Tuncer, and the control horns were created by Bob Wiley.

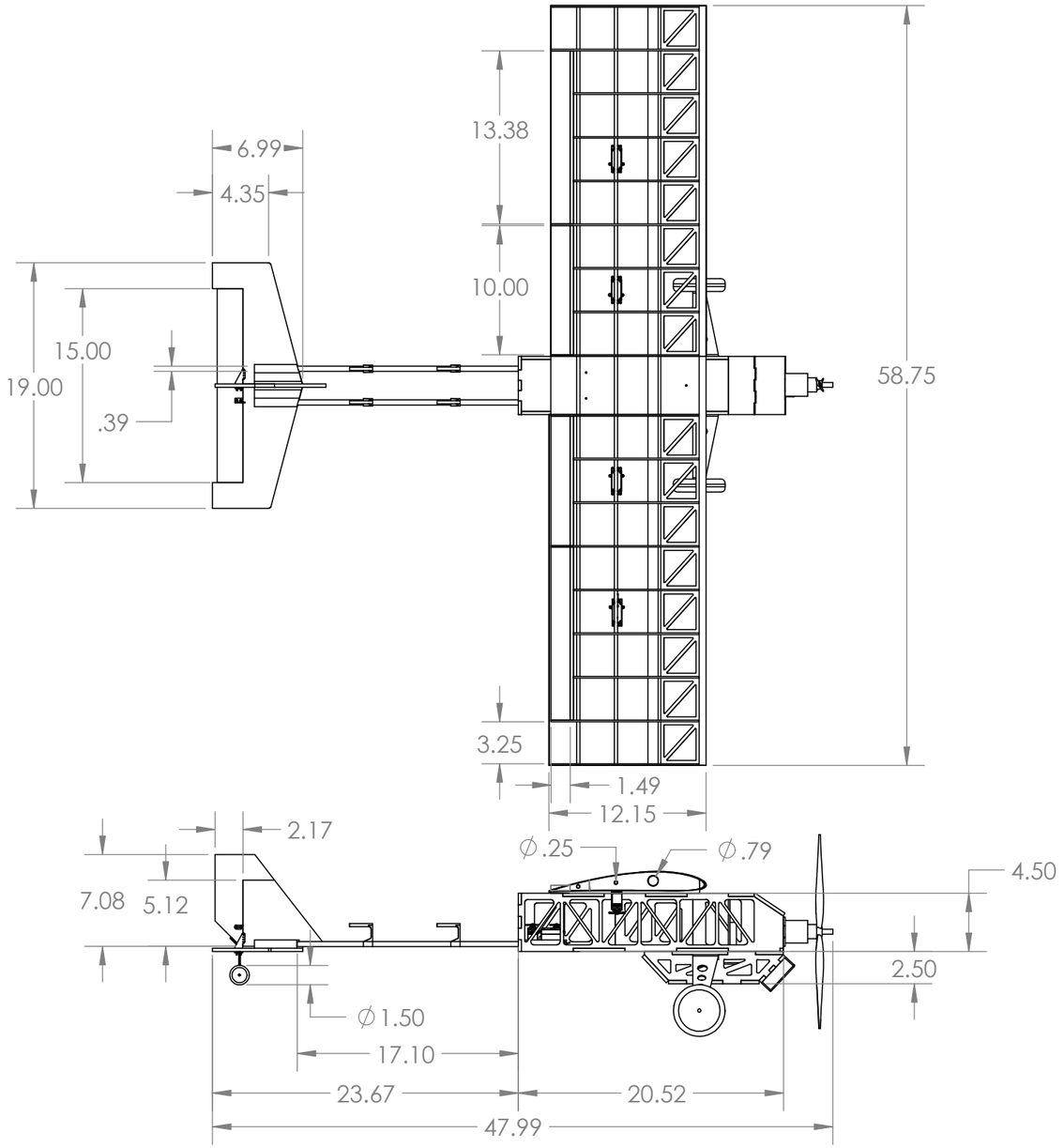

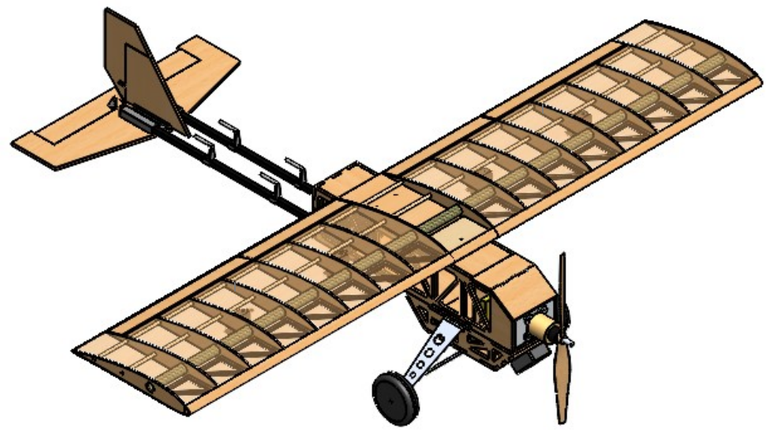

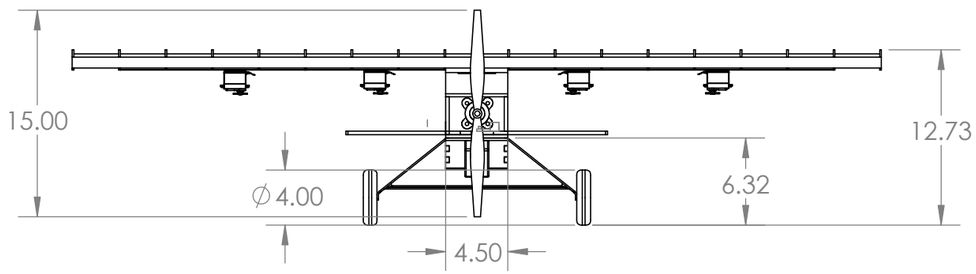

UNLESS OTHERWISE SPECIFIED:		
DIMENSIONS ARE IN INCHES TOLERANCES: FRACTIONAL ± ANGULAR: MACH ± BEND ± TWO PLACE DECIMAL ± THREE PLACE DECIMAL ±		
INTERPRET GEOMETRIC TOLERANCING PER:		
MATERIAL		
FINISH	NEXT ASSY	USED ON
DO NOT SCALE DRAWING	APPLICATION	

	NAME	DATE
DRAWN		
CHECKED		
ENG APPR.		
MFG APPR.		
Q.A.		

COMMENTS:
Drawn by Regina Valencia

TITLE:
WPI 2023-2024 "Project Phoenix"

SIZE	DWG. NO.	REV
B	Three-View	

SCALE: 1:11 | WEIGHT: | SHEET 1 OF 4

ITEM NO.	PART NUMBER	DESCRIPTION	QTY.
1	Left Wall	Lauan Plywood	1
2	Right Wall	Lauan Plywood	1
3	Top Wall	Lauan Plywood	1
4	Bottom Wall	Lauan Plywood	1
5	Front Wall P3	Lauan Plywood	1
6	Back Wall P3	Lauan Plywood	1
7	Hatch	Lauan Plywood	2
8	Front Hatch	Lauan Plywood	1
9	Front Hatch Top	Lauan Plywood	1
10	BC Side	Lauan Plywood	2
11	BC Top	Lauan Plywood	1
12	BC Bottom	Lauan Plywood	1
13	BC Back	Lauan Plywood	1
14	BC Front	Lauan Plywood	1
15	Landing Gear	Aluminum	1
16	Landing Gear Wheel	Rubber & Plastic	2
17	ESC	Phoenix Edge 100	1
18	Tail Attachment Fuselage	3D Printed Part (PLA)	1
19	Firewall Aluminum	Aluminum	1
20	Main Battery	Liperior	1
21	Fuselage Tubes	Carbon Fiber Rod	2
22	Tail Attachment piece	3D Printed Part (PLA)	1
23	VerticalTail	Balsa Wood	1
24	Proto1WingAssembly 2	Balsa, Basswood, Birch	1
25	Proto1WingSpar	Carbon Fiber Rod	1
26	Motor	Scorpion SII-4020-540Kv	1
27	DowelBrace	3D Printed Part (PLA)	4
28	Firewall Wood Front	Birch Plywood	1
29	Firewall Wood Side	Birch Plywood	2
30	Bulkhead	Balsa Wood	1
31	15 inch Propeller	XOAR 2309 15x6	1
32	Servo Motor	HS-425BB	6

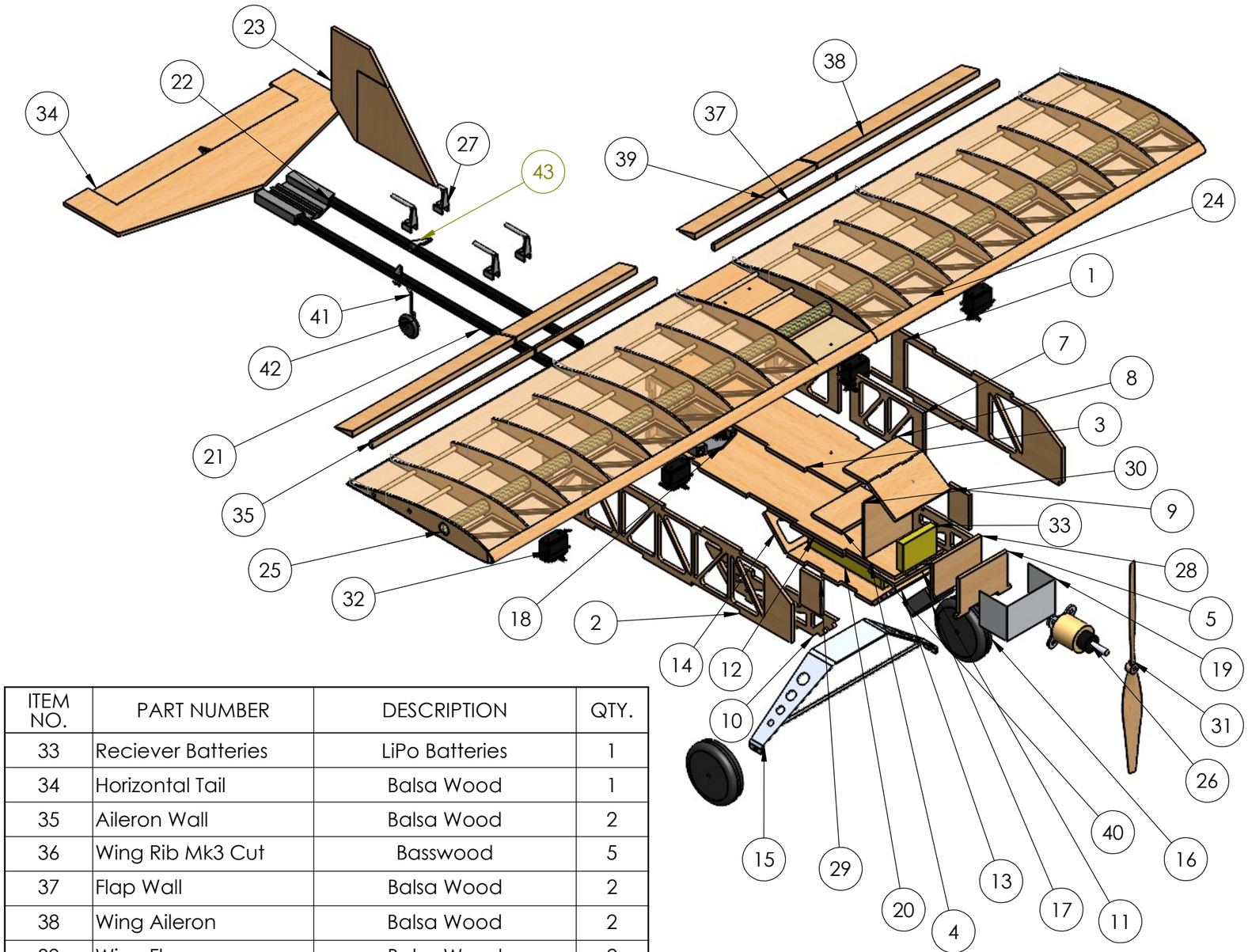

ITEM NO.	PART NUMBER	DESCRIPTION	QTY.
33	Reciever Batteries	LiPo Batteries	1
34	Horizontal Tail	Balsa Wood	1
35	Aileron Wall	Balsa Wood	2
36	Wing Rib Mk3 Cut	Basswood	5
37	Flap Wall	Balsa Wood	2
38	Wing Aileron	Balsa Wood	2
39	Wing Flap	Balsa Wood	2
40	Landing Gear Base	Birch Plywood	1
41	Rear Landing Gear Axle	Aluminum	1
42	Rear Landing Gear Wheel	Foam & Plastic	1
43	Control Horn	Plastic	2

TITLE:

WPI 2023-2024 "Project Phoenix"

SIZE	DWG. NO.	REV
B	Structural View	

SCALE: 1:7 | WEIGHT: | SHEET 2 OF 4

ITEM NO.	PART NUMBER	DESCRIPTION	QTY.
1	Proto1WingSpar	Carbon Fiber Rod	1
2	Wing Rib Mk3	Basswood	8
3	Proto1SmallSpar	Wooden Dowel	2
4	Proto1DTube	Balsa Wood	1
5	Proto1NormalBayBrace	Balsa Wood	16
6	Proto1CenterBrace	Birch Plywood	1
7	Proto1WingSkin	Balsa Wood & Monokote	2
8	Proto1Mount	Birch Plywood	1
9	Wing Rib Mk3 Cut	Basswood	10
10	Servo Motor	HS-425BB	6
11	Aileron Wall	Balsa Wood	2
12	Flap Wall	Balsa Wood	2
13	Wing Aileron	Balsa Wood	2
14	Wing Flap	Balsa Wood	2

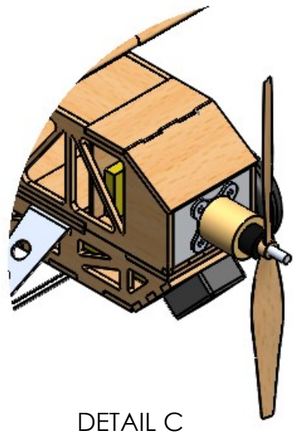

DETAIL C
SCALE 2 : 11

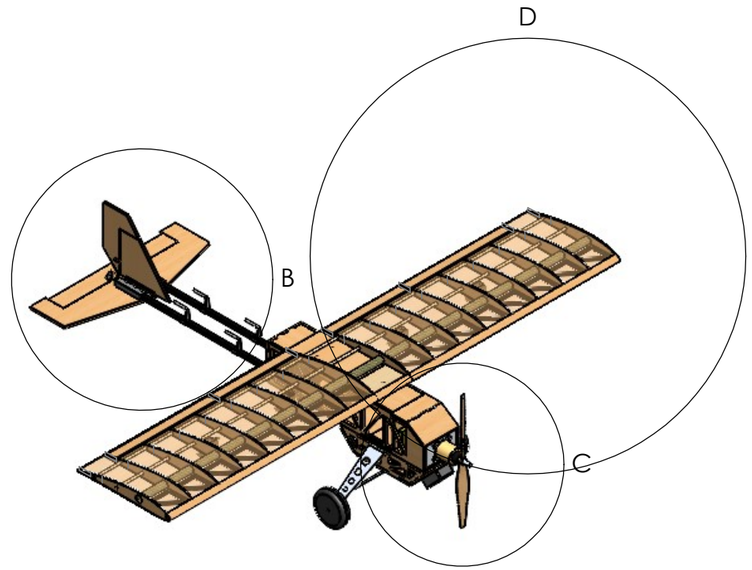

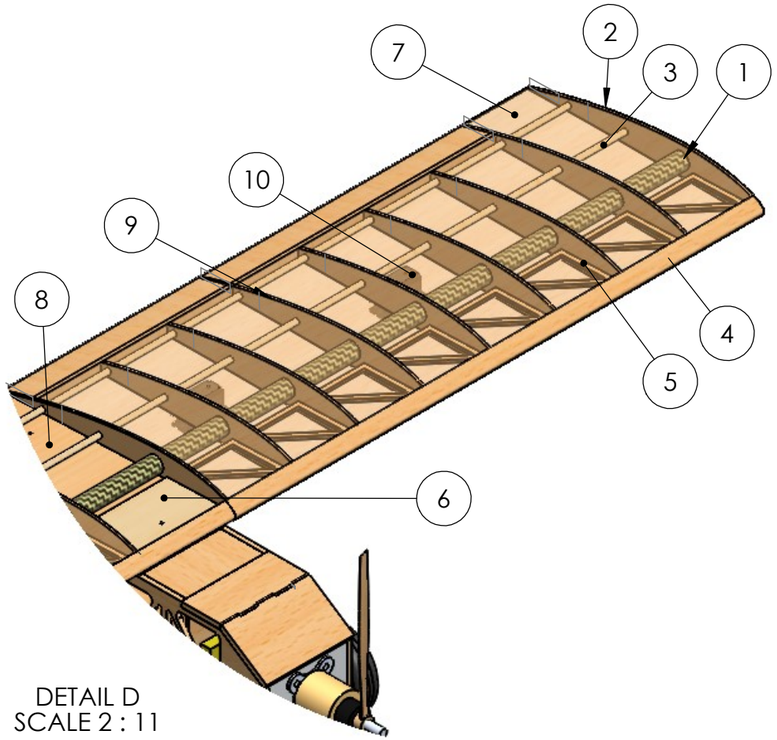

DETAIL D
SCALE 2 : 11

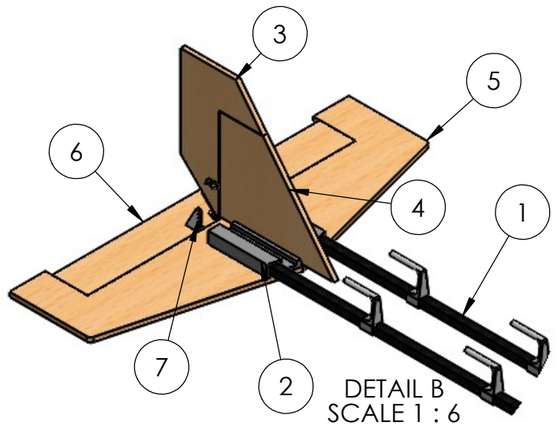

DETAIL B
SCALE 1 : 6

ITEM NO.	PART NUMBER	DESCRIPTION	QTY.
1	Fuselage Tubes	Carbon Fiber Rods	2
2	Tail Attachment piece	3D Printed Custom Part (PLA)	1
3	Rudder	Balsa Wood	1
4	Vertical Stablizer	Balsa Wood	1
5	Horizontal Stablizer	Balsa Wood	1
6	Elevator	Balsa Wood	1
7	Control Horn	Plastic	2

		UNLESS OTHERWISE SPECIFIED:
		DIMENSIONS ARE IN INCHES TOLERANCES: FRACTIONAL ± ANGULAR: MACH ± BEND ± TWO PLACE DECIMAL ± THREE PLACE DECIMAL ±
		INTERPRET GEOMETRIC TOLERANCING PER:
		MATERIAL
NEXT ASSY	USED ON	FINISH
APPLICATION		DO NOT SCALE DRAWING

	NAME	DATE
DRAWN		
CHECKED		
ENG APPR.		
MFG APPR.		
Q.A.		
COMMENTS:		

TITLE:

WPI 2023-2024 "Project Phoenix"

SIZE	DWG. NO.	REV
B	Systems View	

SCALE: 1:16 | WEIGHT: | SHEET 3 OF 4

Crew Insert (Missions 1-3)
Scale: 1:1

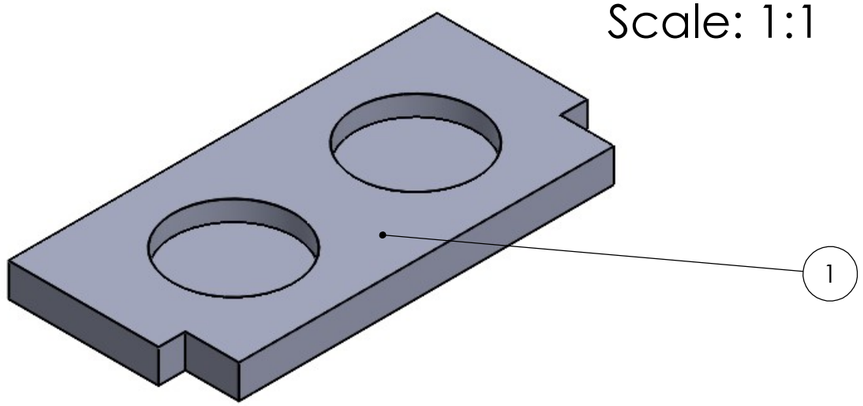

ITEM NO.	PART NUMBER	DESCRIPTION	QTY.
1	Crew Insert	3D Printed Custom Part (PLA)	1

Passenger Insert (Mission 3)
Scale: 1:1.5

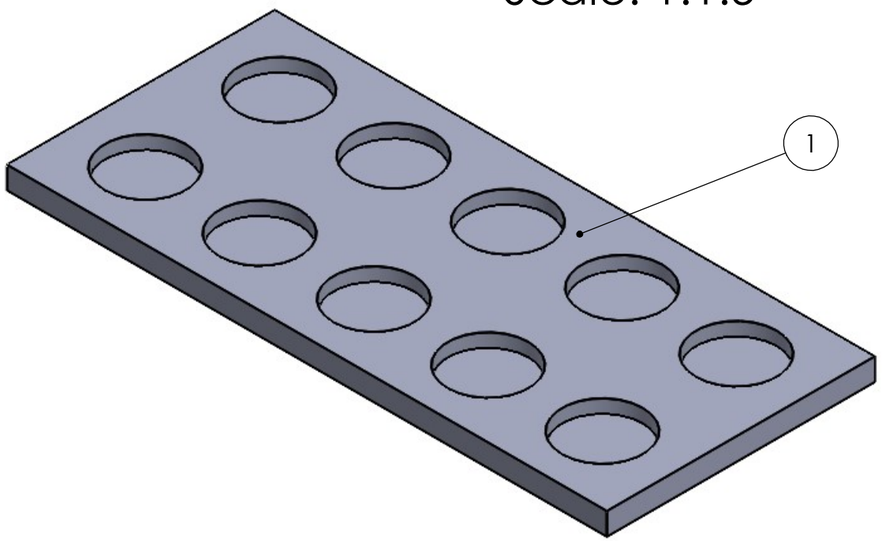

ITEM NO.	PART NUMBER	DESCRIPTION	QTY.
1	Passenger Insert	3D Printed Custom Part (PLA)	1

Payload Inserts (Mission 2)
Scale: 1:1.5

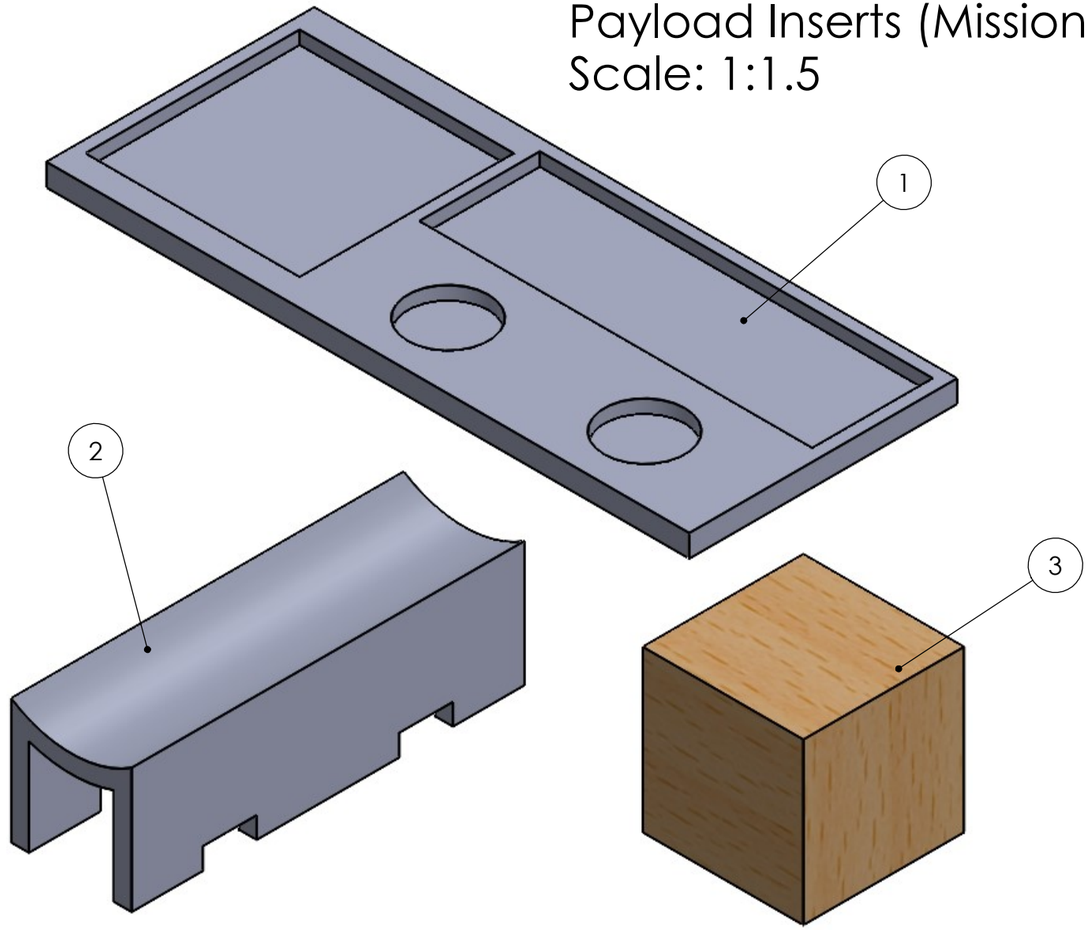

ITEM NO.	PART NUMBER	DESCRIPTION	QTY.
1	Mission 2 Insert	3D Printed Custom Part (PLA)	1
2	Patient Gurney	3D Printed Custom Part (PLA)	1
3	Medical Supply Cabinet	Basswood	1

NEXT ASSY | USED ON

APPLICATION

UNLESS OTHERWISE SPECIFIED:

DIMENSIONS ARE IN INCHES
TOLERANCES:
FRACTIONAL ±
ANGULAR: MACH ± BEND ±
TWO PLACE DECIMAL ±
THREE PLACE DECIMAL ±

INTERPRET GEOMETRIC TOLERANCING PER:

MATERIAL

FINISH

DO NOT SCALE DRAWING

	NAME	DATE
DRAWN		
CHECKED		
ENG APPR.		
MFG APPR.		
Q.A.		

COMMENTS:

TITLE:

WPI 2023-2024 "Project Phoenix"

SIZE	DWG. NO.	REV
B	Payload Accomadations	

SCALE: 1:1 | WEIGHT: | SHEET 4 OF 4